Cell Biology

Sphingolipid imbalance aggravates tau pathology by endomembrane rigidification and rupture

Reviewed Preprint
v1 • May 30, 2025
Not revised

Jessica Tittelmeier, Carl Alexander Sandhof, Nicole Martin, Deike El-Kabarity, Soki-Bradel Ngonza-Nito, Ronald Melki, Carmen Nussbaum-Krammer

Chair of Neuroanatomy, Institute of Anatomy, Faculty of Medicine, Ludwig-Maximilians University of Munich (LMU), Munich, Germany • Center for Molecular Biology of Heidelberg University (ZMBH) and German Cancer Research Center (DKFZ), DKFZ-ZMBH Alliance, Heidelberg, Germany • Chemical Neurobiology Laboratory, Center for Genomic Medicine, Departments of Neurology and Psychiatry, Massachusetts General Hospital and Harvard Medical School, Boston, United States • Institute Francois Jacob (MIRCen), CEA, and Laboratory of Neurodegenerative Diseases, CNRS, Fontenay-Aux-Roses, France

eLife Assessment

This **valuable** study addresses the role of sphingolipid metabolism in maintaining endolysosomal membrane integrity and its impact on tau pathology in *Caenorhabditis elegans* and human cell culture models. The methods are **solid** and the proposed mechanisms are conceivable. However, the current evidence is **incomplete** and could be strengthened, due to reliance on imaging data and insufficient biochemical validation. The work will be of broad interest to cell biologists and biologists working on Alzheimer's disease and related proteinopathies.

https://doi.org/10.7554/eLife.106865.1.sa3

Abstract

Summary

Endolysosomal dysfunction is a hallmark of Alzheimer’s disease (AD) and related tauopathies, yet underlying mechanisms remain poorly understood. This study investigates the role of sphingolipid metabolism in maintaining endolysosomal membrane integrity and its impact on tau aggregation and toxicity in *Caenorhabditis elegans* and human cell culture models. Fluorescence recovery after photobleaching and C-Laurdan dye imaging revealed that silencing sphingolipid metabolism genes reduced endolysosomal vesicle membrane fluidity, increasing their rupture. The accumulation of aggregated tau in endolysosomal vesicles further aggravated endomembrane rigidification and damage and promoted seeded tau aggregation, potentially by facilitating the escape of tau seeds from the endolysosomal system. Supplementation with unsaturated fatty acids improved membrane fluidity, suppressing endolysosomal rupture and seeded tau aggregation in cell models, and alleviating tau-associated neurotoxicity in *C. elegans*. This study provides mechanistic insights into how impaired sphingolipid homeostasis drives endolysosomal membrane

damage and contributes to the progression of tau pathology, suggesting that restoring membrane fluidity may offer a therapeutic strategy for AD.

Introduction

The gradual accumulation of microtubule-associated protein tau (MAPT/tau) aggregates is a hallmark of Alzheimer's disease (AD) and related tauopathies. Misfolded tau species exhibit prion-like behavior by self-replicating and spreading from cell to cell[1,2]. This contributes to the progression of pathology and neurotoxicity, eventually culminating in widespread neuronal dysfunction and degeneration[3]. At the molecular level, tau aggregates replicate by templating the conversion of native tau into an amyloid conformation, promoting its accumulation into fibrillar aggregates. For this to occur at the cellular level, seeding-competent tau species (or tau "seeds") must be released from a donor cell and taken up into the cytosol of the neighboring receiving cell in order to come into direct contact with the cytosolic native tau protein[4–6].

In this process, the autophagy-lysosomal pathway (ALP), which is an important clearance route for tau[7], appears to play a central role. Studies have demonstrated impaired ALP function in the brains of tauopathy patients as well as in animal and cell models, showing that the accumulation of abnormal autolysosomal and endolysosomal vesicles correlating with neuronal toxicity[8–11]. Inhibition of autophagic clearance of tau increases its secretion and spreading[12]. In addition, the accumulation of misfolded tau within endolysosomes leads to a destabilization and rupture of these vesicles[13–18]. While intact endolysosomes normally restrict tau seeds from reaching cytosolic monomers, membrane rupture allows their escape. Recent studies highlight this escape as a critical rate-limiting step in seeded tau propagation[13–18]. Endolysosomal damage not only promotes the propagation of pathological aggregates, but also causes the release of hydrolytic enzymes into the cytosol, leading to cellular damage and death[19]. Although recent efforts to identify pathways involved in endolysosomal damage and repair have intensified, many aspects of these processes remain unknown.

To identify cellular factors that are critical for the integrity of endolysosomal vesicles, we recently performed an unbiased genome-wide RNAi screen in *C. elegans*[20]. One of the pathways identified was sphingolipid (SL) metabolism. SLs constitute a large and diverse class of lipids that are involved in various physiological processes[21,22]. They consist of two main building blocks, a long-chain base with a serine backbone and an attached long acyl chain. This characteristic chemical structure mediates unique biophysical properties. SL biosynthesis and degradation rely on a specialized enzymatic machinery distinct from that of other lipids[23] (**Figure 1A**). Functionally, SLs, along with glycerolipids and sterols, serve as structural components of cell membranes, contributing to the stability and fluidity of membranes and to the organization of microdomains such as lipid rafts. Beyond their structural role, SLs serve as bioactive molecules participating in cellular signaling pathways that control cell growth, differentiation, apoptosis, and intercellular communication[24]. Abnormalities in SL metabolism have been observed during aging and in neurodegenerative conditions, including AD, underscoring their potential significance in the pathogenesis of these disorders[25,26]. Interestingly, recent evidence suggests that sphingolipid accumulation disturbs the endolysosomal pathway and induces or potentiates endolysosomal membrane rupture[27,28]; however, the mechanisms underlying membrane destabilization remain unclear.

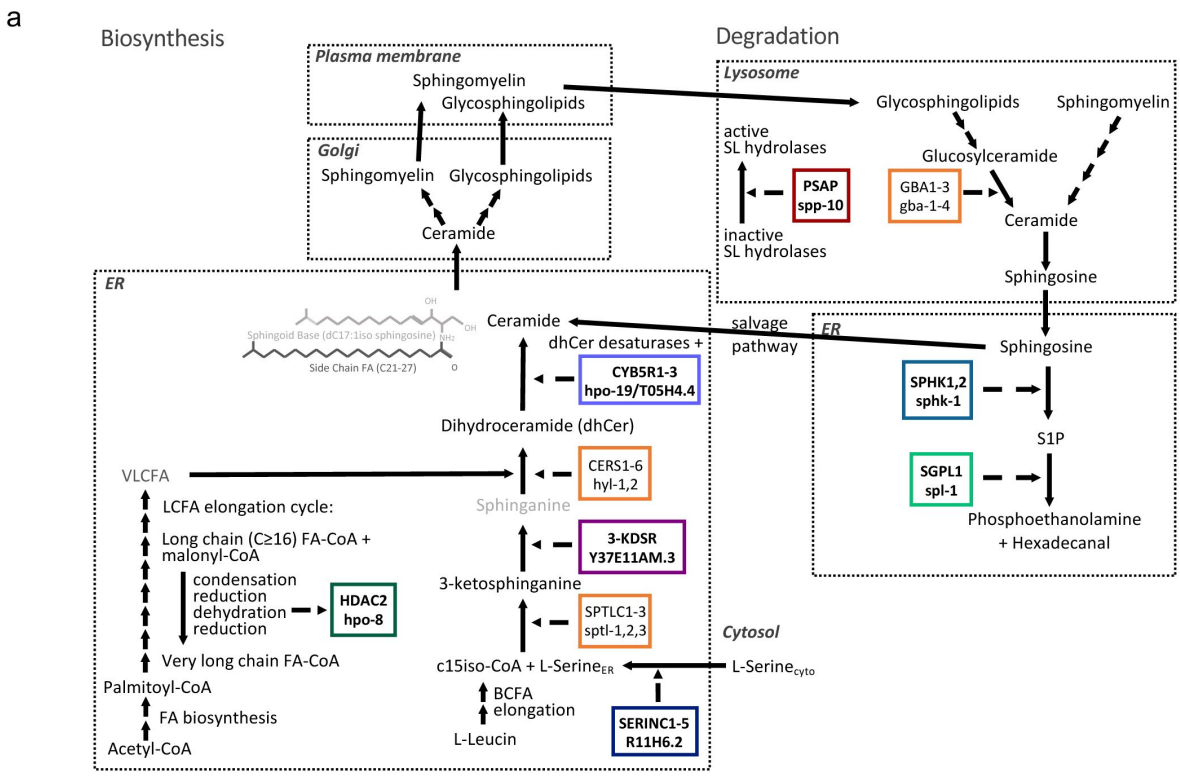
a
Biosynthesis
Degradation
Plasma membrane
Sphingomyelin
Glycosphingolipids
Golgi
Sphingomyelin
Glycosphingolipids
Ceramide
Lysosome
Glycosphingolipids
Sphingomyelin
active
SL hydrolases
PSAP
spp-10
Glucosylceramide
GBA1-3
gba-1-4
Ceramide
inactive
SL hydrolases
Sphingosine
ER
Sphingoid Base (dC17:1iso sphingosine)
Side Chain FA (C21-27)
Ceramide
salvage
pathway
ER
Sphingosine
dhCer desaturases +
CYB5R1-3
hpo-19/T05H4.4
SPHK1,2
sphk-1
Dihydroceramide (dhCer)
S1P
SGPL1
spl-1
VLCFA
CERS1-6
hyl-1,2
Sphinganine
Phosphoethanolamine
+ Hexadecanal
LCFA elongation cycle:
Long chain (C≥16) FA-CoA +
malonyl-CoA
3-KDSR
Y37E11AM.3
condensation
reduction
dehydration
reduction
HDAC2
hpo-8
3-ketosphinganine
SPTLC1-3
sptl-1,2,3
Very long chain FA-CoA
Cytosol
c15iso-CoA + L-Serine$_{ER}$
L-Serine$_{cyto}$
Palmitoyl-CoA
BCFA
elongation
FA biosynthesis
L-Leucin
SERINC1-5
R11H6.2
Acetyl-CoA

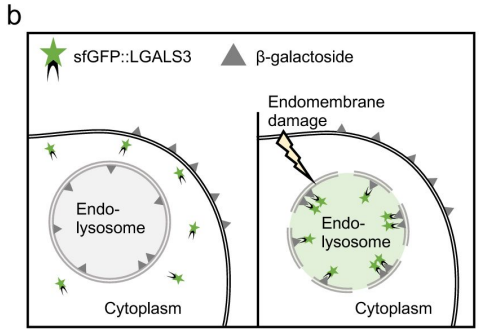
b
sfGFP::LGALS3
β-galactoside
Endomembrane
damage
Endo-
lysosome
Endo-
lysosome
Cytoplasm
Cytoplasm

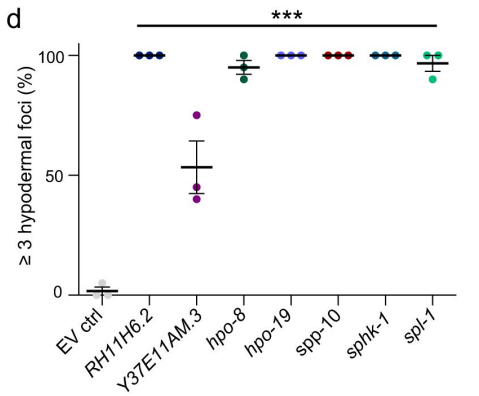
d
***
≥ 3 hypodermal foci (%)
100
50
0
EV ctrl
RH11H6.2
Y37E11AM.3
hpo-8
hpo-19
spp-10
sphk-1
spl-1

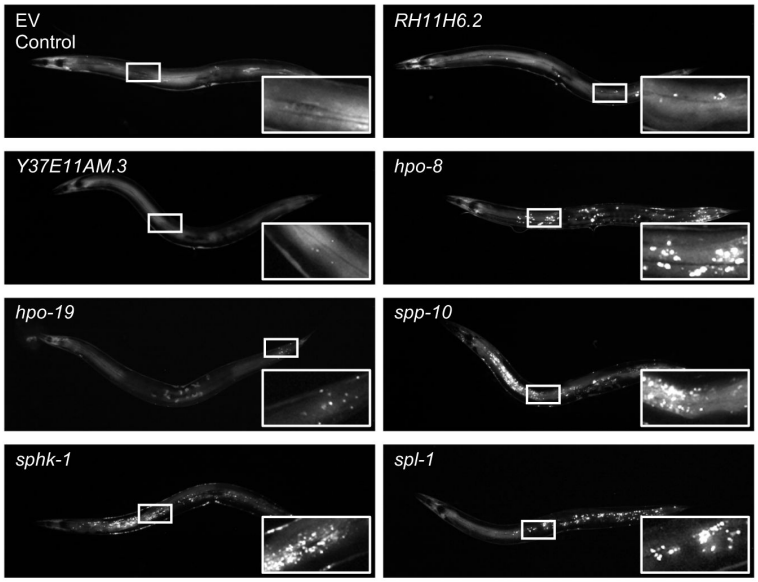
c
EV
Control
RH11H6.2
Y37E11AM.3
hpo-8
hpo-19
spp-10
sphk-1
spl-1

Figure 1.

Sphingolipid metabolism dysregulation by KD is linked to of endolysosomal vesicle rupture.

(**A**) General overview of sphingolipid metabolism with a particular focus on the genes identified in the screen we performed. Sphingolipids constitute a group of amphipathic lipids featuring a polar head group and a sphingoid base backbone that is N-acetylated with a (very) long-chain fatty acid ((V)LCFA) side chain. In contrast to mammals, where the sphingoid base is conventionally derived from palmitic acid and serine, *C. elegans* sphingolipids usually contain a characteristic C17iso branched chain sphingoid base [68–70]. Its synthesis involves the branched chain FA (BCFA) elongation pathway to yield C15iso-CoA, which then condensates with L-serine to form 3-ketosphinganine. This reaction is catalyzed by serine palmitoyltransferase (encoded by *sptl-1*, *–2*, and *-3*). The serine incorporator (SERINC) protein family (encoded by *R11H6.2*) is believed to assist in the incorporation of L-serine into specific membranes. 3-ketodihydrosphingosine reductase (KDSR, in *C. elegans* predicted to be encoded by Y37E11AM.3) then catalyzes the reduction of 3-keto sphinganine to sphinganine. The (V)LCFA side chain is primarily comprised of a straight saturated FA chain, ranching from 20-26 carbon atoms in length, with or without hydroxylation [30,71]. It can be also derived from BCFAs, such as C15iso and C17iso [68,69]. However, most of the side chain FA moieties originate from palmitoyl-CoA via the canonical de novo FA biosynthesis pathway, involving the sequential addition of C2 moieties from malonyl-CoA through the LCFA elongation cycle [68,69]. Each elongation cycle comprises four reactions (condensation, reduction, dehydration, reduction), with the third reaction requiring very-long-chain (3R)-3-hydroxyacyl-CoA dehydratase (encoded by *hpo-8*) [69]. Finally, ceramide synthases (encoded by *hyl-1* and *hyl-2*) catalyze the addition of various acyl side chains to the sphingoid base to yield dihydroceramide, which is then desaturated to ceramide. The latter reaction is catalyzed by dihydroceramide desaturases, which require electrons from NAD(P)H provided by cytochrome b5 reductases (encoded by *hpo-19* and *T05H4.4*). All complex sphingolipids, such as sphingomyelin and glycosphingolipids (including cerebrosides and gangliosides) originate from ceramide. Degradation of complex sphingolipids takes place in the lysosome. Essential for this process are saposins or sphingolipid activator proteins (PSAPs, encoded by *spp-10*), which serve as crucial bridges between the lipid substrate and hydrophilic hydrolases. Glucocerebrosidases (encoded by *gba-1*, *gba-2*, *gba-3*, and *gba-4*) hydrolyse glucosylceramide into ceramide and glucose. Sphingosine may be either recycled and metabolized back into ceramide or phosphorylated by sphingosine kinase (encoded by *sphk-1*) to generate sphingosine-1-phosphate (S1P). S1P lyase (encoded by *spl-1*) irreversibly cleaves S1P into phospho-ethanolamine and hexadecenal. The *C. elegans* genes identified in the primary screen, along with their human orthologs, are framed with color. Genes identified in subsequent co-RNAi experiments and their human orthologs are framed in gray.

(**B**) Schematic of lysosomal rupture detected by the galectin puncta assay.

(**C**) Widefield fluorescence images of animals expressing hypodermal sfGFP::LGALS3. Numerous foci are visible upon RNAi-mediated KD of sphingolipid metabolisms genes. Zoomed in image is indicated in overview image by a white box.

(**D**) Mean percentage of animals positive for lysosomal rupture (defined as three or more sfGFP::LGALS3 foci in the hypodermis). Data shown as means of three technical replicate plates with 17-30 animals per plate ± SEM. Statistical analysis comparing RNAi conditions to the empty vector control (EV ctrl) was done using one-way ANOVA with Dunnett's post-hoc test. *** = $p < 0.001$.

Here we investigated the role of SL metabolism in the maintenance of endolysosomal vesicle integrity. Our results revealed that silencing of SL metabolism genes led to a marked reduction in membrane fluidity, particularly in endolysosomal vesicles, thereby increasing their fragility and rupture. The accumulation of aggregated tau had an additive effect and led to a further reduction in endomembrane fluidity, which aggravated the damage to the endolysosomal compartment.

Increased membrane rigidity also facilitated seeded tau aggregation. Improvement of membrane fluidity through supplementation of polyunsaturated fatty acids (PUFAs) counteracted tau propagation in cells and tau-associated neurotoxicity in *C. elegans*.

This study highlights the interplay between lipid metabolism and proteostasis and provides insights into how disturbances in sphingolipid homeostasis contribute to endolysosomal dysfunction and tau pathology. In addition, it provides a possible mechanistic explanation for the beneficial effect of PUFA supplementation that has been observed in AD patients and suggests that restoring membrane fluidity may help mitigate tau toxicity and disease progression.

Results

Knockdown of sphingolipid metabolism genes induces lysosomal rupture

Several of the strongest hits identified in the unbiased genome-wide RNAi screen we performed to identify modulators of endolysosomal vesicles integrity were genes involved in SL metabolism (**Figure 1A**). Knockdown (KD) of these genes (the serine incorporator *R11H6.2*, the 3-ketodihydrosphingosine reductase *Y37E11AM.3*, the hydroxyacyl-CoA dehydratase *hpo-8*, the cytochrome b5 reductases *hpo-19* and *T05H4.4*, the saposin *spp-10*, the sphingosine kinase *sphk-1*, and the sphingosine-1-phosphate lyase *spl-1*) via RNA interference (RNAi) induced endolysosomal membrane damage as detected by a galectin puncta assay[29] (**Figure 1B-D**). Under steady-state conditions, human galectin-3 fused to superfolder-GFP (sfGFP::LGALS3) exhibits an even distribution within the cytosol of hypodermal cells. Upon endolysosomal vesicle damage and exposure of their lumen to the cytosol, sfGFP::LGALS3 binds exposed β-galactoside and re-localizes, yielding visible puncta[29].

The screen identified distinct steps in sphingolipid metabolism catalyzed by non-redundant genes or targeted by a single RNAi clone, as in the case of *hpo-19*/*T05H4.4* which are both depleted by *hpo-19* RNAi. However, other steps in this pathway, which are mediated by two or more proteins may have been missed in the screen. Indeed, simultaneous KD of selective redundant genes using co-RNAi revealed additional genes functioning in *de novo* sphingolipid biosynthesis that also induced endolysosomal rupture, including the serine palmitoyltransferases *sptl-1* and *–3* and the ceramide synthases *hyl-1* and *–2* (Figure S1A). In addition, the co-KD of all four glucocerebrosidases *gba-1-4* or only *gba-2-4*, also triggered endolysosomal rupture (Figure S1B). Hence, these findings suggest that the KD of genes involved in both biosynthesis and degradation of SLs contributes to endolysosomal rupture, highlighting the tightly regulated nature of sphingolipid metabolism. Any disruption in this balance poses challenges to endolysosomal integrity.

KD of sphingolipid metabolism genes particularly affects membrane fluidity of endolysosomal vesicles

SLs are important components of eukaryotic cell membranes and genetic modulation of SL metabolism likely affects the lipid composition and biophysical properties of membranes. Similar to their mammalian isoforms, the N-acyl chains of *C. elegans* SLs contain predominantly long and saturated fatty acid chains[30,31], which tend to pack tightly within the lipid bilayer. As such, a higher proportion of SLs generally reduces membrane fluidity, leading to increased order, rigidity, or viscosity[32]. Consequently, KD of the hits involved in SL degradation should lead to SL accumulation and reduced membrane fluidity, while KD of the hits involved in SL biosynthesis should have the opposite effect.

To evaluate the membrane fluidity of endolysosomal membranes, fluorescence recovery after photobleaching (FRAP) was employed on *C. elegans* that express the Lysine/Arginine Transporter 1 (LAAT-1) tagged with mCherry, which localizes to the lysosomal membrane[33]. FRAP enables the assessment of the lateral mobility of LAAT-1 within the lysosomal membrane, thereby indirectly measuring its fluidity. We focused our analysis on the hypodermis, where we expressed the sfGFP::LGALS3 reporter and observed endolysosomal rupture following KD of the SL metabolism genes (**Figure 1C**, D). Interestingly, KD of all of our hits significantly increased the time required to recover half of the maximum fluorescence intensity (t_{half}), indicating less fluid lysosomal membrane in the hypodermis (**Figure 2A-C**, E, F). With some gene KDs, we also observed a decrease in the maximal recovered signal after bleaching (**Figure 2D**, G). The decrease in lysosomal membrane fluidity was not specific to the hypodermis as the KD of *spl-1* also increased the t_{half} of LAAT-1::mCherry in intestinal lysosomes (Figure S2A-D). To discern whether the detrimental effect of KD on membrane fluidity is confined to lysosomal membranes or extends to other cellular membranes, we utilized a *C. elegans* strain expressing a plasma membrane-anchored GFP[34]. Intriguingly, this reporter showed no change in the t_{half} with any KD and only *spl-1* KD led to decrease in the maximal recovered signal (**Figure 2H-K**). Hence, the endolysosomal membrane seems to be particularly sensitive to a disruption of SL metabolism in contrast to the plasma membrane. Dysregulation of both, synthesis and degradation of SLs reduces the fluidity of the endolysosomal membrane and makes it more susceptible to rupture.

KD of sphingolipid metabolism genes affects membrane fluidity in human cells

Next, we asked whether dysregulation of SL metabolism exerts similar effects in human cells. To this end, we employed HEK293T cells and C-Laurdan dye to evaluate membrane fluidity (**Figure 3A**). This approach leverages the unique properties of C-Laurdan, which emits fluorescent light of varying wavelengths in response to changes within the phospholipid bilayer, particularly reflective of membrane fluidity[35,36]. The shift in emission profile between liquid-disordered and liquid-ordered phases allows a quantitative assessment of the membrane order by calculating the ratiometric relationship of the fluorescence intensity recorded in two spectral channels, known as a generalized polarization (GP) value[35] (**Figure 3A**). Decreasing GP values are indicative of increasingly fluid membrane while increasing GP values denote increased rigidity. Of note, we exposed the cells to C-Laurdan for an extended time of 2 hours (instead of 30 min as recommended in the original protocol), to promote internalization of the dye and thus increase the staining of endolysosomal membranes relative to the plasma membrane[35]. Upon KD of *SPHK2*, one of the human homologs of the *C. elegans sphk-1* gene, the C-Laurdan fluorescence GP ratio augmented significantly, indicating increased membrane rigidity (**Figure 3B**, D and Figure S3A). Of note, Lipofectamine 2000 was used to deliver siRNA into the cells and lipid-based transfection reagents have been shown to impact endolysosomal membranes[37]. Indeed, Lipofectamine alone slightly increased membrane fluidity (**Figure 3C**). Taken together, FRAP and C-Laurdan analyses revealed that disrupted SL homeostasis led to more ordered and rigid endolysosomal membranes, in both *C. elegans* and human cells.

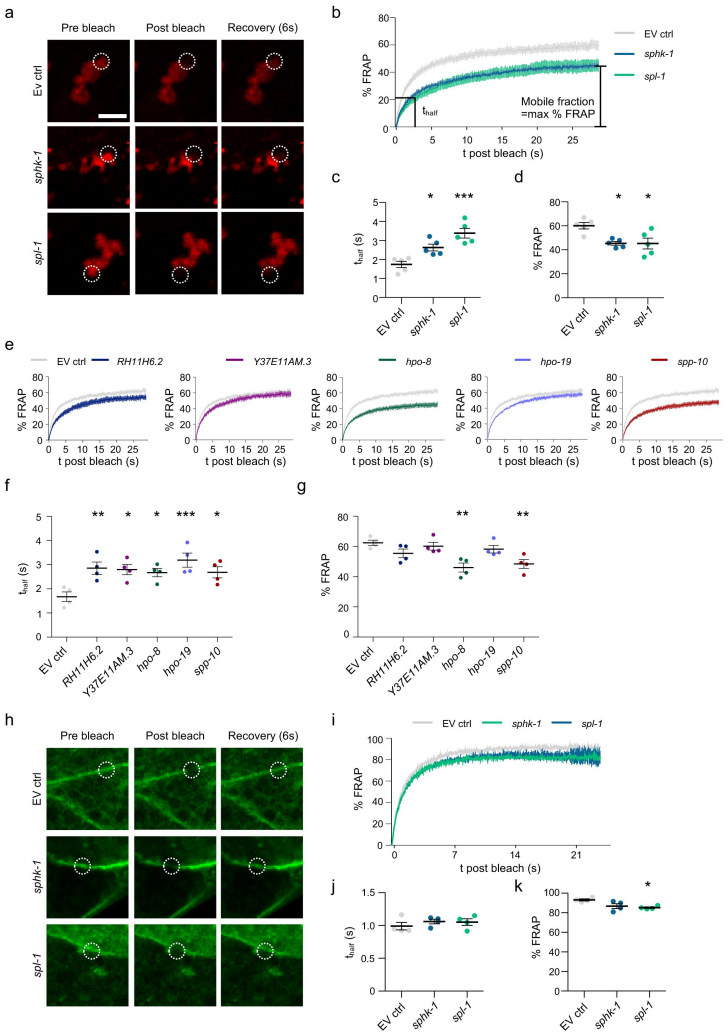

Figure 2.

Knockdown of genes involved in sphingolipid metabolism decreases lysosomal membrane fluidity.

(A) Representative confocal single plane images from a FRAP experiment in animals expressing a mCherry tagged Lysosomal Lysine/Arginine Transporter 1 (LAAT-1::mCherry) in the hypodermis grown either on empty vector control (EV ctrl), *spl-1* or *sphk-1* RNAi plates. Dashed circles outline the bleach spots.
(B) Combined FRAP curves of LAAT-1::mCherry in hypodermal lysosomal membranes. Curves are normalized to the pre-bleach intensity as 100% and the first post-bleach intensity as 0%.
(C, D) Increase (C) in the mean time until half of the maximal signal is recovered (t_{half},) and decrease (D) in the maximal % recoverable fluorescence values upon KD of *sphk-1* and *spl-1* indicate a reduction in lysosomal membrane fluidity.
(**E**) FRAP curves of LAAT-1::mCherry in hypodermal lysosomal membranes of animals grown either on empty vector or the indicated RNAi plates. Curves are normalized to the pre-bleach intensity set as 100% and the first post-bleach intensity as 0%.
(**F**) Mean t_{half} upon KD of sphingolipid metabolism genes.
(**G**) Maximal % recoverable fluorescence values upon KD of sphingolipid metabolism genes.
(**H**) Representative confocal single plane images from a FRAP experiment in animals expressing prenylated GFP for lipid membrane anchorage in the intestine.
(**I**) Combined FRAP curves of prenylated GFP enriched on the intestinal plasma membrane of animals grown either on empty vector, *sphk-1* or *spl-1* RNAi plates. Curves are normalized to the pre-bleach intensity as 100% and the first post-bleach intensity as 0%.
(J, K) Mean t_{half} (J) and maximal % recoverable fluorescence values (K). Data represented as means ± SEM of 5 – 12 FRAP measurements per condition collected in five biological replicates. Statistical analysis comparing RNAi conditions to the empty vector control was done using one-way ANOVA with Dunnett's post-hoc test. n.s.: not significant, * = $p < 0.05$, ** = $p < 0.01$, *** = $p < 0.001$

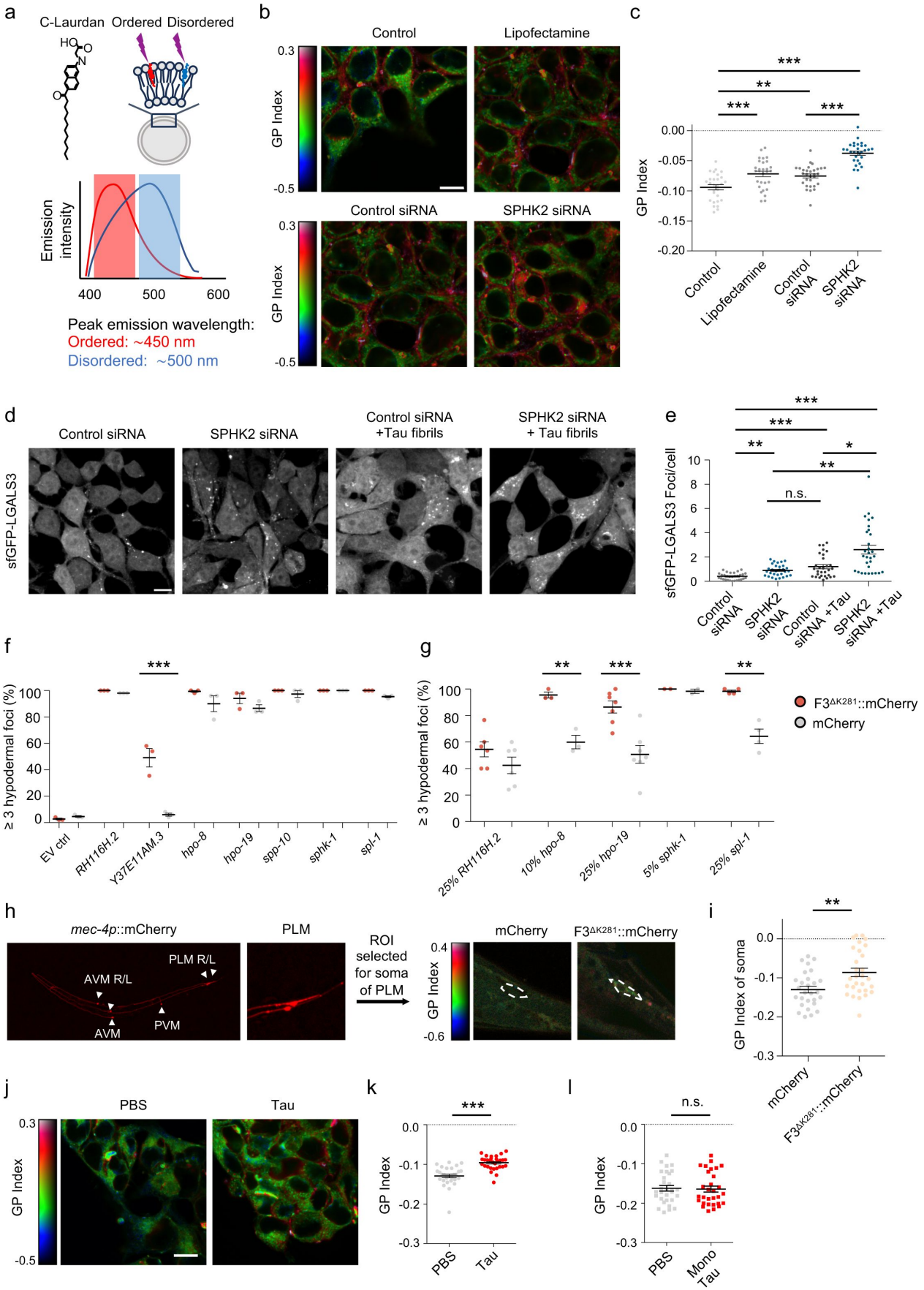
a
C-Laurdan Ordered Disordered
HO
O
N
O
Emission intensity
400
500
600
Peak emission wavelength:
Ordered: ~450 nm
Disordered: ~500 nm
b
Control
Lipofectamine
Control siRNA
SPHK2 siRNA
GP Index
0.3
-0.5
c
GP Index
0.00
-0.05
-0.10
-0.15
-0.20
***
**
***
***
Control
Lipofectamine
Control siRNA
SPHK2 siRNA
d
Control siRNA
SPHK2 siRNA
Control siRNA +Tau fibrils
SPHK2 siRNA + Tau fibrils
sfGFP-LGALS3
e
sfGFP-LGALS3 Foci/cell
10
8
6
4
2
0
***
***
**
*
**
n.s.
Control siRNA
SPHK2 siRNA
Control siRNA +Tau
SPHK2 siRNA +Tau
f
≥ 3 hypodermal foci (%)
100
80
60
40
20
0
***
EV ctrl
RH116H.2
Y37E11AM.3
hpo-8
hpo-19
spp-10
sphk-1
spl-1
g
≥ 3 hypodermal foci (%)
**
***
**
F3ΔK281::mCherry
mCherry
25% RH116H.2
10% hpo-8
25% hpo-19
5% sphk-1
25% spl-1
h
mec-4p::mCherry
PLM
PLM R/L
AVM R/L
AVM
PVM
ROI selected for soma of PLM
mCherry
F3ΔK281::mCherry
GP Index
0.4
-0.6
i
GP Index of soma
0.0
-0.1
-0.2
-0.3
**
mCherry
F3ΔK281::mCherry
j
PBS
Tau
GP Index
0.3
-0.5
k
GP Index
0.0
-0.1
-0.2
-0.3
***
PBS
Tau
l
GP Index
0.0
-0.1
-0.2
-0.3
n.s.
PBS
Mono Tau

Figure 3.

KD of SPHK2 and aggregated tau reduces membrane fluidity leading to lysosomal rupture.

(A) Scheme of the fluorescence properties of C-Laurdan. The dye is excited using illumination at 405 nm. The dye fluoresces with a peak emission wavelength around 450 nm (red) when residing in the ordered phase and ~500 nm in the disordered phase (blue). Two-channel acquisition is conducted in the wavelength bands indicated by shaded boxes.

(B) Pseudo-color images showing the GP index of C-Laurdan dye at each pixel position in HEK293T cells upon KD of SPHK2.

(C) Increase in GP Index of HEK293T cells upon KD of SPHK2. Statistical analysis was done using one-way ANOVA with Bonferroni's post-hoc test.

(D) Max. intensity projection of confocal z-stacks of HEK293T cells expressing sfGFP-LGALS3 upon KD of SPHK2 and seeding with 1N4R tau fibrils.

(E) Average number of foci per number of cells. n= 3 independent experiments, 10 images each. Statistical analysis done using oKruskal-Wallis with a Dunn's post-hoc test.

(F) Quantification of the percentage of animals with ≥ 3 hypodermal sfGFP::LGALS3 foci, representing endolysosomal damage, expressing either the F3$^{\Delta K281}$::mCherry (red) or only the mCherry tag (grey) in touch receptor neurons under knockdown of the indicated genes.

(G) Dilution of the indicated RNAi cultures with the empty vector control culture was done to reduce the strength of the knockdown. Data represented as mean ± SEM. Besides knockdown of *sphk-1* in **C** n = 3 – 7 with **F** 40 – 50 or **G** 20 – 30 animals per replicate. Since even a dilution down to 5% of the *sphk-1* RNAi resulted in 100% of animals being scored as positive in two independent replicates this condition was not repeated further. Statistical analysis comparing RNAi conditions to the empty vector control done using one-way ANOVA with Dunnett's post-hoc test.

(H) Worms expressing F3$^{\Delta K281}$::mCherry or mCherry in touch receptor neurons stained with C-Laurdan. The mCherry signal was used to select a region of interest (ROI) around the soma of the posterior touch receptor neurons (PLM) to determine the GP Index.

(I) Increase in rigidity of membranes in animals expressing F3$^{\Delta K281}$::mCherry compared to mCherry. Statistical analysis was done using a t-test. n=4, total of at least 28 worms.

(J) Pseudocolored HEK293T cells exposed to tau 1N4R fibrils visualizing the C-Laurdan dye GP Index.

(K) Increase rigidity of membranes of cells seeded with tau fibrils as indicated by the GP index.

(L) GP index of cells seeded with monomeric tau. Statistical analysis for C-Laurdan in cells was done using a t-test. n= 3 independent experiments, 10 images each. Scale bar 10 µm. n.s.: not significant, * = $p < 0.05$, ** = $p < 0.01$, *** = $p < 0.001$.

Fibrillar tau increases membrane rigidity and exacerbates endolysosomal damage

To investigate whether disruption of SL homeostasis also affects endolysosomal integrity in human cells, we generated a HEK293T cell line stably expressing the same sfGFP-LGALS3 reporter used for the galectin puncta assay in *C. elegans*. To further mimic the *C. elegans* model, in which aggregation-prone tau fragments are chronically transferred from the touch receptor neurons into the hypodermis where the sfGFP-LGALS3 reporter is expressed[20], recombinant 1N4R tau fibrils were added to sfGFP-LGALS3 expressing HEK293T cells on top of the KD of *SPHK2*. Interestingly, both the addition of tau fibrils alone and the KD of *SPHK2* alone already caused rupture of endolysosomes in sfGFP-LGALS3 cells (**Figure 3D**, E and Figure S3B). The combination of both had an additive effect (**Figure 3D**, E and Figure S3B).

We therefore asked whether the KD of SLs alone would also already rupture hypodermal endolysosomes in *C. elegans* and whether accumulation of transmitted tau would exacerbate this process. To answer this question, we determined the amount of hypodermal sfGFP-LGALS3 foci in $F3^{\Delta K281}$::mCherry *C. elegans* compared to control animals expressing only the mCherry tag. KD of *Y37E11AM.3* alone did not increase lysosomal rupture compared to the EV control RNAi, only the presence of tau spreading resulted in more lysosomal rupture relative to the control (**Figure 3F**). KD of the remaining hits resulted in near 100% animals with hypodermal sfGFP-LGALS3 foci in both the $F3^{\Delta K281}$::mCherry and mCherry control strains. To test whether the additional negative impact of the F3 tau fragment might be masked by the strength of the RNAi clones, different dilutions of the RNAi bacteria were tested. Under conditions where the RNAi KD did not saturate the readout of the assay, KD of *spl-1*, *hpo-8*, and *hpo-19* alone already affected lysosomal integrity (**Figure 3G**). Moreover, $F3^{\Delta K281}$::mCherry transgenic animals showed a significantly higher level of endolysosomal rupture upon KD of *spl-1*, *hpo-8*, and *hpo-19* compared to the mCherry control (**Figure 3G**). Diluting the *R11H6.2* RNAi clone showed no significant differences, and KD of *sphk-1* still resulted in 100% endolysosomal rupture-positive animals in both genetic backgrounds even after dilution of the RNAi bacteria to below 5% and could therefore not be assessed. In conclusion, chronic transmission of the $F3^{\Delta K281}$::mCherry fragment from the touch receptor neurons to the hypodermis impaired the endolysosomal system exacerbating the rupture due to perturbation of SL homeostasis.

Since disruption of SLs metabolism led to an increase in membrane rigidity resulting in endolysosomal rupture, and fibrillar tau also ruptured endolysosomal membranes (**Figure 3D**, E)[14], we asked whether tau itself could also affect membrane fluidity. To test this, membrane fluidity was assessed for somas of the posterior (PLM) touch receptor neurons of *C. elegans* using C-Laurdan dye. Indeed, expression of the tau fragment led to a decrease in membrane fluidity compared to expression of the mCherry tag alone (**Figure 3H**, I). Also, HEK293T cells incubated with tau fibrils for 5 hours exhibited an increased GP index (**Figure 3J**, K). Importantly, this was specific to fibrillar tau, as monomeric tau had no effect on membrane fluidity (**Figure 3L** and Figure S3C). Thus, aggregated forms of tau can cause rigidification of the endolysosomal membrane, resulting in increased fragility and rupture.

Membrane rigidification exacerbates seeded tau aggregation

The packing of fatty acids within the membrane influences membrane fluidity. Saturated fatty acids (SFAs) have straight hydrocarbon chains forming a tightly packed, highly ordered and rigid membrane. To investigate the role endomembrane lipid homeostasis plays in tau propagation, we introduced an SFA to rigidify membranes. Incubating HEK293T cells with the SFA palmitic acid (PA) conjugated to BSA increased membrane rigidity (**Figure 4A**, B). In addition, cells incubated with PA and tau fibrils had an even more rigid membrane than cells incubated with tau fibrils alone (**Figure 4C**, D).

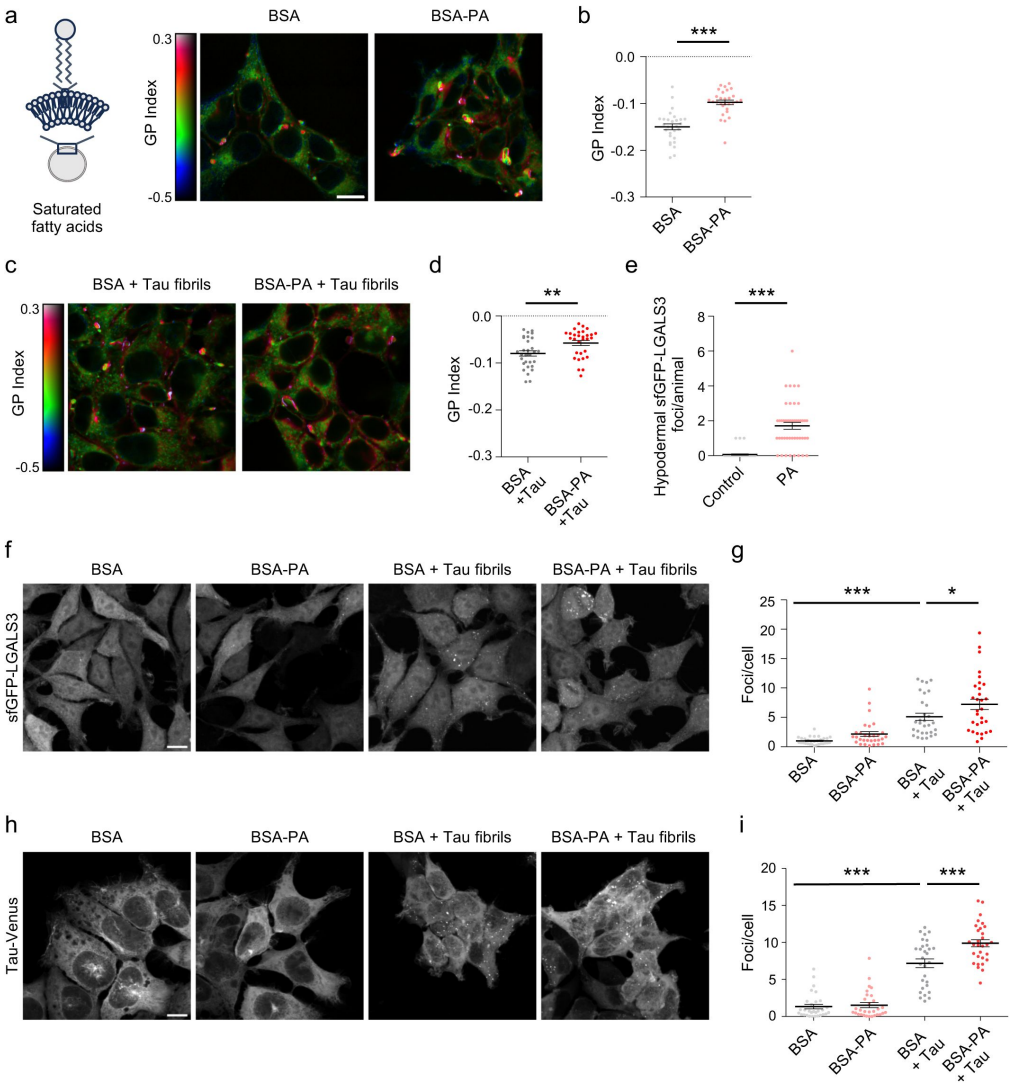

Figure 4.

Saturated fatty acids decrease membrane fluidity and exacerbate seeded tau aggregation.

(A) Left: saturated fatty acid membrane scheme. Right: pseudocolored HEK293T cells pre-loaded with 50 µM PA conjugated to BSA (BSA-PA) displaying the C-Laurdan dye GP Index.
(B) GP Index indicates increased rigidity of membranes with BSA-PA. Statistical analysis was done using the Mann-Whitney-test. n= 3 independent experiments, 10 images each.
(C) Pseudocolored HEK293T cells pre-loaded with BSA-PA and seeded with 1N4R tau fibrils.
(D) GP Index indicates an additive impact of tau fibrils on membrane rigidity when added to HEK293T cells pre-loaded with BSA-PA. Statistical analysis was done using t-test. n= 3 independent experiments, 10 images each.
(E) Quantification of hypodermal sfGFP-LGALS3 foci in animals grown on plates supplemented with PA reveal an increase in lysosomal rupture. Statistical analysis was done using Mann-Whitney test. n= 3 independent experiments, 15 worms per replicate.
(F) Max. intensity projection of confocal z-stacks of HEK293T cells expressing sfGFP-LGALS3 pre-loaded with BSA-PA and seeded with 1N4R tau fibrils.
(G) Quantification of sfGFP-LGALS3 foci in HEK293T cells following indicated treatments.
(H) Max. intensity projection of confocal z-stacks of Venus-tagged full-length P301S tau biosensor cells pre-loaded with BSA-PA and seeded with 1N4R tau fibrils.
(I) Quantification of Venus-P301S tau foci following indicated treatments. Statistical analysis comparing BSA + tau to other conditions was done using one-way ANOVA with Dunnett's post-hoc test. n= 3 independent experiments, 10 images each. * = $p < 0.05$, ** = $p < 0.01$, *** = $p < 0.001$. Scale bar 10 µm.

An important step in tau propagation is tau seeds escape from the endolysosomal compartment, which can then propagate themself by recruiting native monomeric tau. Therefore, we asked if the PA-induced loss of membrane fluidity impairs endolysosomal integrity. Worms grown on plates supplemented with PA displayed an increase in endolysosomal rupture (**Figure 4E**). In cells, the addition of PA alone did not lead to endolysosomal rupture; however due to compounding impact of PA and tau fibrils on membrane fluidity, the addition of PA increased fibrillar tau-induced endolysosomal rupture (**Figure 4F**, G). Hence, loss of membrane fluidity mediated by fibrillar tau and/or SFAs negatively affects endolysosomal integrity, resulting in increased endolysosomal rupture.

Impairment of endolysosomal integrity may enhance tau propagation as tau could escape from the endolysosomal compartments, reach the cytosol and recruit native monomeric tau, promoting seeded tau aggregation. Given the observed membrane rigidification after pre-loading with SFAs, we investigated whether membrane lipid composition influences tau propagation using a tau biosensor cell line expressing Venus-tagged full-length P301S mutant 0N4R tau (tau-Venus)[38,39]. PA-induced membrane rigidification led to an increase in tau-Venus foci upon seeding with tau fibrils (**Figure 4H**, I). Moreover, KD of *SPHK2* also increased the formation of tau-Venus foci due to SPHK2 KD-mediated membrane rigidification (Figure S4C, D). This highlights a positive correlation between membrane rigidity and seeded tau aggregation. Changes in membrane fluidity, which compromise endolysosomal integrity may promote the entry of seeds into the cytosol. This would consequently foster the seeded propagation of tau aggregation.

Increasing membrane fluidity by PUFAs rescues neurotoxic phenotypes

Given that membrane stiffening exacerbates tau propagation, we wondered whether we could prevent this by improving membrane viscosity. While SFA allow for tightly packed lipids, unsaturated fatty acids have one or more double bonds in their hydrocarbon chain that introduce kinks in their structure, resulting in loosely packed lipids and increased membrane fluidity. Therefore, we investigated whether we could rescue tau pathology using polyunsaturated fatty acids (PUFAs). Incubating HEK293T cells with the ω-3 PUFA α-linolenic acid (ALA) increased membrane fluidity (**Figure 5A** and Figure S5A). Moreover, pre-loading with ALA prevented tau-induced membrane rigidification and decreased the GP-index of membranes even after the addition of tau fibrils (**Figure 5B**, C). Importantly, pre-loading cells with ALA also counteracted fibrillar tau-mediated endolysosomal rupture (**Figure 5D**, E and Figure S5B).

Since ALA prevented endolysosomal rupture, we expected it to also prevent seeded tau aggregation. Indeed, tau-Venus cells pre-loaded with ALA exhibited significantly fewer foci when exposed to tau fibrils (**Figure 5F** and Figure S5C). These data show that ALA supplementation counteracts tau-mediated decrease in membrane fluidity, thereby preventing endolysosomal rupture and decreasing seeded tau aggregation.

Finally, we asked whether ALA would also reduce the toxicity associated with aggregated tau. Expression of $F3^{\Delta K281}$::mCherry in touch receptor neurons resulted in an age-dependent decline in the response to gentle touch from day 4, corresponding to the first day of adulthood to day 8, corresponding to day 5 of adulthood (**Figure 5H**, and Figure S5D)[20]. Addition of ALA to the growth medium mitigated this loss of function (**Figure 5H** and Figure S5D) and also reduced neurotoxicity (**Figure 5I**, J). Thus, supplementation with ALA not only reduced endolysosomal damage but also attenuated neurotoxic phenotypes associated with aggregated tau.

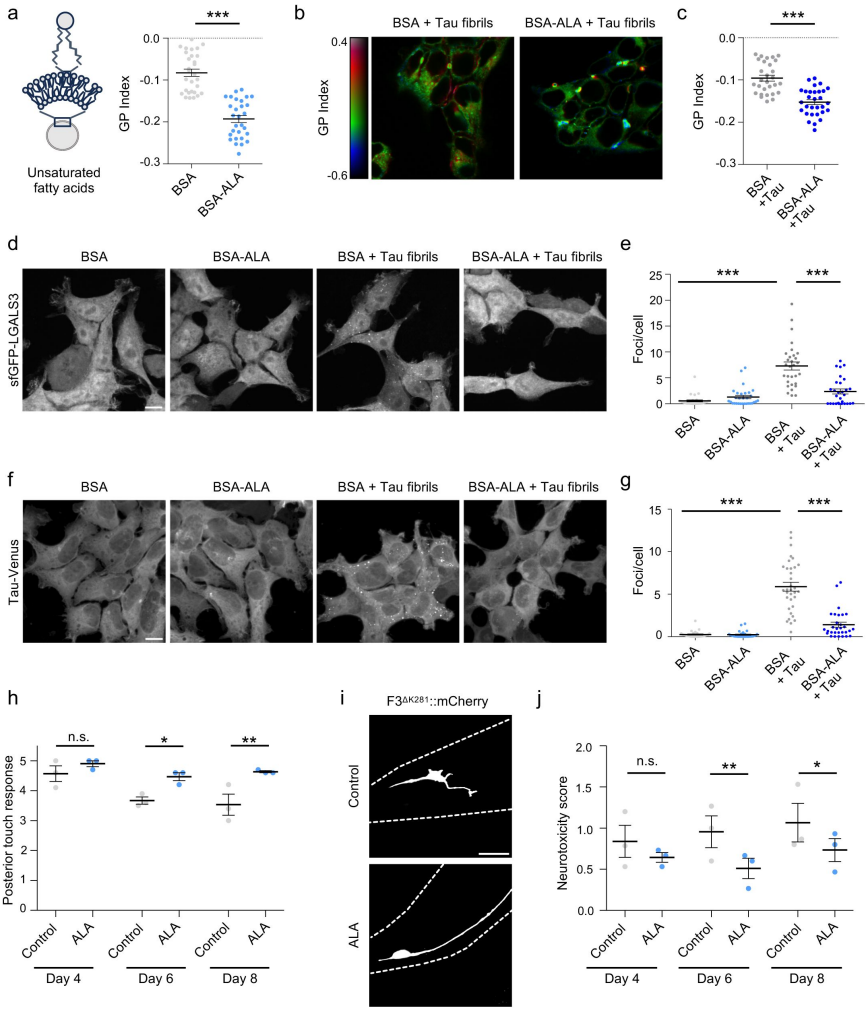

Figure 5.

PUFA supplementation restores lysosomal membrane integrity and reduces seeded tau aggregation and toxicity.

(A) Left: unsaturated fatty acid membrane scheme. Right: C-Laurdan GP Index of HEK293T cells pre-loaded with 150 µM ALA conjugated to BSA (BSA-ALA) indicating an increase in membrane fluidity. Statistical analysis was done with a t-test. n= 3 independent experiments, 10 images each.
(B) Pseudocolored HEK293T cells pre-loaded with BSA-ALA and seeded with 1N4R tau fibrils.
(C) GP Index indicates that BSA-ALA reduces tau-induced rigidification of the membrane. Statistical analysis was done using the Mann-Whitney U-test. n= 3 independent experiments, 10 images each.
(D) Max. intensity projection of confocal z-stacks of HEK293T cells expressing sfGFP-LGALS3 pre-loaded with BSA-ALA and seeded with 1N4R tau fibrils. Scale bar 10 µm.
(E) Quantification of sfGFP-LGALS3 foci following indicated treatments. n= 3 independent experiments, 10 images each.
(F) Max. intensity projection of confocal z-stacks of tau-Venus biosensor cell line pre-loaded with BSA-ALA and seeded with 1N4R tau fibrils. Scale bar 10 µm.
(G) Quantification of tau-Venus foci following indicated treatments. Statistical analysis comparing BSA + tau to other conditions was done using Kruskal-Wallis with Dunn's post-hoc test. n = 3 independent experiments, 10 images each.
(H) Posterior response to touch during aging of animals expressing $F3^{\Delta K281}$::mCherry grown on plates supplemented with ALA or only the ethanol solvent. Statistical analysis was done using two-way ANOVA with Bonferroni's multiple comparison test.
(I) Max. intensity projection of confocal z-stacks of day 6 old animals expressing $F3^{\Delta K281}$::mCherry.
(J) Neurotoxicity score of PLM neurons of animals grown on control or ALA plates. Statistical analysis was done using 2-way ANOVA with a Holm-Sidak's multiple comparison test. n= 3 independent experiments, 15 worms per replicate. Scale bar 20 µm. * = $p < 0.05$, ** = $p < 0.01$, *** = $p < 0.001$.

Discussion

In a previous genome-wide screen in *C. elegans*, we identified genes involved in SL metabolism as crucial for maintaining endolysosomal integrity[20]. In this study we explored the mechanisms by which disruption of SL homeostasis leads to endolysosomal rupture and how it affects tau pathology. We found that imbalanced SL metabolism leads to decreased membrane fluidity, and subsequent endolysosomal rupture. This promoted seeded tau aggregation in a biosensor cell line exposed to fibrillar tau, implying that dysregulation of SL metabolism might boost disease progression by enhancing propagation of tau aggregation.

The central nervous system (CNS) is particularly rich in lipids. Approximately 50% of the brain's dry weight consists of lipids with high concentrations of cholesterol, phospholipids and sphingolipids [40,41]. Alterations in lipid and SL metabolism have been observed not only during the aging process, but also in various late-onset neurodegenerative diseases including AD[26,42]. While aging is the major risk factor for AD, one of the most significant genetic risk factors for AD is the apolipoprotein E (ApoE) polymorphism, specifically the ApoE4 allele[43]. ApoE is the primary lipoprotein in the brain, crucial for lipid transport and metabolism. Besides cholesterol, the ApoE4 variant has been shown to influence SL metabolism, thereby affecting the pathogenesis of AD from its early stages[26,42,44]. While disturbances in SL homeostasis are increasingly recognized as a contributing factor to the onset and progression of the disease[26,42], the underlying mechanisms are poorly understood.

Our results show that reducing the expression of genes involved in both, biosynthesis and degradation of SLs significantly reduced the fluidity of endolysosomal membranes, making them more fragile and prone to rupture. KD of the saposin *spp-10*, the sphingosine kinase *sphk-1*, and the sphingosine-1-phosphate lyase *spl-1* blocks the degradation of complex SLs and should lead to an increase in their relative abundance, and therefore to a decrease in membrane fluidity. KD of the very-long-chain (3R)-3-hydroxyacyl-CoA dehydratase *hpo-8*, which is involved in fatty acid elongation, has been demonstrated to promote the incorporation of long-chain UFAs into phospholipids, thereby restoring plasma membrane fluidity[45]. The absence of *hpo-8* leads to membrane rigidification[45]. Conversely, KD of the serine incorporator *R11H6.2* and the 3-ketodihydrosphingosine reductase *Y37E11AM.3*, which function in the SL de novo synthesis pathway, should theoretically decrease total SL content and consequently increase membrane fluidity. The cytochrome b5 reductases *hpo-19* and *T05H4.4*, required for lipid desaturation, are involved in the conversion of dihydroceramide to ceramide and the biosynthesis of PUFAs[46]; KD of these genes is expected to reduce the levels of SLs and PUFAs, which could theoretically either increase or decrease membrane fluidity, depending on which metabolic pathway is predominantly affected.

Our observation that KD of all these genes results in decreased membrane fluidity is seemingly counterintuitive. However, SLs form a complex metabolic network and can interconvert, allowing a dynamic adaptation of SL levels. In addition, the cell likely compensates for the loss of certain SLs by increasing the biosynthesis of other lipid molecules. This dynamic interplay makes it difficult to predict how individual genes affect the endolysosomal membrane lipid composition. Genes that are involved in apparently opposing steps of SL metabolism could therefore still lead to an accumulation of similar SL species.

Future lipidomic analyses are necessary to determine the SL and lipid content of endolysosomal membranes in our model systems. Such studies will provide a clearer understanding of how genetic manipulation of SL metabolism affects endomembrane lipid composition and could pinpoint the exact species likely responsible for the observed membrane rigidification.

AD brains exhibit elevated levels of sphingosine, ceramide 1-phosphate, and ceramide compared to control subjects[42]. Multivariate analysis and machine learning also identified these SL species as key contributors to AD[42]. These and other analyses were performed in different brain regions but without cell type or subcellular resolution. We found that disruption of *C. elegans* SL homeostasis primarily affected endolysosomal membranes and had little effect on plasma membrane fluidity. The lysosomal membrane is particularly rich in sphingolipids[47], which seems to make it more susceptible to disruption of SL homeostasis. Studies in yeast have shown that increased membrane lipid saturation affects the vacuole —the functional counterpart of mammalian lysosomes—as well as the nuclear envelope, whereas the plasma membrane and mitochondria remained relatively unaffected[48]. These findings indicate that cellular membranes vary in their resilience to lipid saturation stress, potentially due to differences in lipid composition and protective mechanisms[48,49]. To better understand the implications of SL alterations in AD, it would be important to examine whether the observed changes primarily originate from endolysosomal membranes or also from other organelles, such as the endoplasmic reticulum and the nucleus, or from the plasma membrane.

Intriguingly, expression of the aggregation-prone F3 tau fragment also enhanced membrane rigidity with SL homeostasis disruption having an additive effect, exacerbating endomembrane damage. Thus, alterations in SL metabolism could be not only a cause but also a consequence of AD related pathology[26,42]. The accumulation of misfolded tau in lysosomes could impair the lysosomal clearance capacity. This dysfunction may reduce the activity of acid hydrolases, leading to an accumulation of biomolecules, including membrane lipids. Impairment of membrane lipid metabolism could in turn further compromise lysosomal integrity and function. Both processes – accumulation of SLs and protein aggregates – may create a vicious self-promoting cycle of lysosomal dysfunction that eventually leads to neurodegeneration.

Supplementation of SFAs exacerbated the negative impact of the F3 tau fragment on endomembrane fluidity. Given the high levels of saturated and trans fats in the Western diet[50], it is plausible that dietary factors also contribute to the dysregulation of lipid homeostasis in the brain. The Mediterranean UFA-rich diet has been associated with healthy aging, while reduced UFA brain levels have been correlated with increased tau and Aβ pathology and decreased cognitive function in AD[51,52]. Restoring membrane fluidity through the supplementation of PUFAs mitigated tau propagation in cells and reduced tau-associated neurotoxicity in *C. elegans*. These results suggest a potential mechanism for the beneficial effects of PUFA supplementation observed in AD patients[53,54]. Future studies are needed to evaluate whether these benefits are related to an increase in the fluidity of endolysosomal membranes and the consequent prevention of their damage by protein aggregates and/or impaired SL homeostasis.

In sum, this study revealed an important role of endolysosomal membrane homeostasis in disease progression providing a possible mechanism for the detrimental effect of SL imbalance and beneficial effect of PUFA supplementation that have been observed in AD patients.

Methods

Maintenance of *C. elegans* and age synchronization

All animals were cultured using standard methods[55]. If not otherwise indicated, worms were grown on nematode growth medium (NGM) plates seeded with *E. coli* strain OP50 at 20 °C. For RNAi, NGM medium were supplemented with Ampicillin, Tetracycline, and IPTG, seeded with the respective HT115 *E. coli* RNAi clones and grown at 20 °C. Animals were age-synchronized by bleaching. Briefly, gravid adults were dissolved in 20% sodium hypochlorite solution. The surviving *C. elegans* embryos were hatched overnight in M9 buffer with gentle rocking at 20 °C. The next day, appropriate amounts of L1 larvae were added to the plates.

C. elegans fatty acid supplementation

Polyunsaturated fatty acids were dissolved in EtOH and stored in the dark at –20 °C under a N_2 atmosphere to prevent oxidation. NGM was cooled after autoclaving to 55 °C. To enhance fatty acid distribution, NP-40 substitute (0.001% v/v) was added to the media and subsequently either 0.3 mM of the desired fatty acid solution or the ethanol solvent as control and stirred for 5 min before plate pouring [56]. Palmitic acid (PA) was supplemented by enriching the OP50 bacterial food source. Overnight cultures were grown in the presence of 2 mM of PA dissolved in EtOH or EtOH. The next day, OP50 bacteria were pelleted by centrifugation (10 min at 4500x g) and washed 2x with M9 buffer[57]. 10x concentrated bacteria (in M9) were then seeded on NGM plates.

Quantification of lysosomal rupture (galectin puncta assay) in *C. elegans*

Quantification of animals showing hypodermal lysosomal rupture was done as previously described[29,58]. Briefly, age-synchronized animals expressing the sfGFP::LGALS3 construct in the hypodermis were seeded on OP50 or RNAi NGM plates. Scoring was done using a Leica M205 FA widefield binocular microscope. 20-50 worms were analyzed per replicate.

Mounting of live animals for imaging

Synchronized animals were mounted on 8-10% agarose in M9 buffer pads with a drop of mounting mix (2% (w/v) levamisole and 50% (v/v) nanosphere size standards (Thermo Fisher)) and covered with a coverslip.

Fluorescence recovery after photobleaching (FRAP)

FRAP measurements to estimate membrane fluidity were done following a published protocol[59]. Animals were synchronized by bleaching and grown until the second day of adulthood on the indicated RNAi or empty vector (EV) control plates. Directly before the FRAP experiments, animals were mounted at the Zeiss LSM 780 confocal microscope. FRAP measurements of either GFP enriched in the intestinal plasma membrane, or LAAT-1::mCherry located in intestinal or hypodermal lysosomal membranes were taken with 40X Water immersion objective. For the lysosomal membrane, mCherry-positive membranes were photobleached over a circular area (seven pixel radius) using 10 iterations of the 561 nm DPSS laser with 100% laser power transmission. Images were collected at a 12-bit intensity resolution over 128 × 128 pixels (digital zoom 6X) using a pixel dwell time of 3.15 µsec with 2% laser power transmission. For the plasma membrane, GFP-positive membranes were photobleached over a circular area (10 pixel radius) using 20 iterations of the 488 nm Argon laser with 100% laser power transmission. Images were collected at a 12-bit intensity resolution over 128 × 128 pixels (digital zoom 6X) using a pixel dwell time of 3.15 µsec with 10% laser power transmission. At least 6 pre-bleaching images were collected before the region of interest was bleached. The recovery of fluorescence was traced for 25s. Fluorescence recovery and T_{half} were calculated as previously described in Svensk et al.[60].

Touch sensory assay and neurotoxicity in touch receptor neurons

Touch sensory assay was done as previously described[61]. Briefly, touch sensitivity was tested by gently stroking the tip of an eyebrow hair attached to a toothpick transversely across the anterior or posterior half of an animal. A touch-sensitive animal was one that stopped/moved away from the stimulus. 10 worms were examined for each strain in 3 biological replicates with 5 strokes in the anterior and posterior. For neurotoxicity scoring of the PLM neurons, live animals were imaged using an Olympus IXplore SpinSR Confocal microscope with an UplanS Apo 60x/1.30 Silicon oil objective. The neurotoxicity score was determined by adding a score of 1 for each of the following phenotypes: soma outgrowth, process branching, process break, wavy process. 15 animals were examined at each day of age in 3 independent biological replicates.

Cell culture

Cells were cultured in DMEM containing high glucose, GlutaMAX Supplement, pyruvate (Gibco), and 10% FBS (Gibco) at 37 °C and 5% CO_2. Regular mycoplasma tests were performed (GATC Biotech). HEK293T cells expressing Venus-tagged full-length P301S mutant 0N4R tau (0N4R tauP301S-Venus) were kindly provided by Dr. William A. McEwan, Cambridge University[38].

Cloning of mammalian expression constructs and generation of sfGFP-LGALS3 HEK293T cells

HEK293T cells were cultured in DMEM containing high glucose, GlutaMAX supplement, pyruvate (Gibco), and 10% FBS (Gibco) at 37 °C and 5% CO_2. Cells expressing sfGFP-LGALS3 were generated as follows. sfGFP::LGALS3 was amplified from the *C. elegans* expression plasmid pPD49.26 by PCR and cloned into the pLenti PGK Puro DEST (w529-2) vector backbone (Addgene plasmid #19068) by MultiSite Gateway cloning according to the manufacturers protocol. pLenti PGK Puro DEST (w529-2) was a gift from Eric Campeau & Paul Kaufman[62]. After each cloning step plasmids isolated from bacterial colonies grown on selective media were extracted with the GenEluteTM Five-Minute Plasmid Miniprep Kit (Qiagen) and validated by sequencing. HEK293T sfGFP-LGALS3 were generated using a 3rd generation lentiviral system. Lentivirus was produced by transiently transfecting HEK293T cells with the pLenti PGK Puro DEST, MDL-gagpol, RSV-REV and IVS-VSVG at a ratio of 5:3:1:1, respectively. Cell media was changed 24 hours after transfection. Viral supernatant was collected 72 h post-transfection. After centrifugation at 2000 x g for 5 min, the supernatant containing the virus was concentrated by adding the PEG-it Virus Precipitation Solution (Systems Biosciences) followed by overnight incubation at 4 °C. The precipitated virus was pelleted by centrifugation (1500 x g, 30 min, 4°C), resuspended in DMEM containing 25 mM HEPES buffer and stored at –80 °C. The lentivirus was added to HEK293T followed by treatment with Puromycin to select successfully transduced HEK293T cells stably expressing sfGFP-LGALS3.

Quantification of lysosomal rupture (galectin puncta assay) in cells

Cells were imaged on an Olympus IXplore SpinSR Confocal microscope with an UplanS Apo 60x/1.30 Silicon oil objective. To detect the number of foci in an image, a difference of gaussian blur was applied to max projections to isolate foci from cytsosolic sfGFP signal. Thresholding was applied using 'moments' threshold on FIJI. Number of foci was counted using the 'analyze particles' function. Cell number was counted manually to obtain number of foci/cell for each image.

C-Laurdan dye measurement of membrane fluidity in worms and cells

Live worms were stained with 10 mM C-Laurdan dye (6-dodecanoyl-2-dimethylaminonaphthalene) (Thermo Fisher Scientific) as previously described[63]. Cells were also stained with C-Laurdan at 15 µM for 2 hours then fixed in 4% PFA in PBS. Images were acquired with an DMI6000 confocal microscope and Leica software with a 63x oil-immersion objective, with a zoom factor of 4. Samples were excited with a 405 nm laser and the emission recorded between 400 and 460 nm (ordered phase) and between 470 and 530 nm (disordered phase). Quantitative assessment of the membrane order was achieved by calculating the ratiometric relationship of the fluorescence intensity recorded in two spectral channels (GP value) by using an automated ImageJ macro, according to published guidelines[35].

Knockdown of target genes by RNAi in cells

SPHK2 or a scrambled control siRNA was purchased from Thermo Scientific Dharmacon (ONTarget plus siRNA and Control Pool). Cells were seeded in DMEM with 10% FBS. siRNA was diluted in siRNA buffer (Final concentration 20 nM) before mixing with Lipofectmine2000 for 20 min prior to being added to cells. To minimize lipofectamine impact on the endolysosomal system, media was exchanged after 6 hours.

SDS-Page and immunoblotting

Cells were pelleted by centrifugation followed by lysis in lysis buffer (10mM Tris, 100mM NaCl, 0.2% Triton X-100, 10mM EDTA) on ice for 20 min. The lysates were transferred into fresh Eppendorf tubes and centrifuged (1000 g for 1 min at 4 °C) in a tabletop centrifuge to remove cellular debris. The protein concentration was determined using protein assay dye reagent concentrate (Bio-Rad). Proteins were separated under denaturing conditions by SDS–PAGE and transferred onto a PVDF membrane (Carl Roth) by standard wet blotting protocols. Samples were probed with rabbit polyclonal anti-SPHK2 (1:5000, 9C5E1, Santa Cruz) primary antibody. Anti-GAPDH antibody (1:5000, clone GAPDH-71.1, Sigma-Aldrich) was used as loading control.

HRP-conjugated anti-mouse and anti-rabbit IgG secondary antibodies (Bio-Rad) were used for subsequent ECL-based detection (Bio-Rad).

Fatty acid treatment in cells

For α-linolenic acid (ALA), a stock solution was made in EtOH and stored in the dark at –20°C under a N_2 atmosphere to prevent oxidation[64]. Palmitic acid (PA) was dissolved in 0.1 M NaOH according to Cousin et al.[65]. ALA and PA were then conjugated to BSA in 10% fatty acid free solution by shaking for 1 hour at 37°C to a concentration of 6 mM for ALA and 5 mM for PA[66]. Prior to preloaded cells with BSA-PA, the solution was heated to 65 °C for 15 min. For assays with C-Laurdan, cells were preloaded with FAs for 3 hours before the addition of C-Laurdan for another 2 hours. If preloading was followed by seeding with tau, preloading with FAs was done for 3 hours before fibrillar tau was added for an additional 5 hours. C-Laurdan was spiked in for the last 2 hours. No media changes were done between steps. For experiments with HEK293T tau-Venus cells and HEK293T sfGFP-LGALS3 cells, preloading with FAs was done for 3 hours before seeding with 1N4R tau fibrils. Cells were then fixed after 48 hours.

Monomeric and fibrillar tau

Full-length human 1N4R tau was expressed and purified as previously described[67]. The purified monomeric tau was dialyzed against PBS buffer containing 1 mM DTT, flash frozen in liquid nitrogen and stored at –80 °C. The concentration of monomeric tau was determined spectrophotometrically using an extinction coefficient at 280 nm of 7575 M^{-1} cm^{-1}. Monomeric 1N4R tau was assembled into fibrils at 40 μM in the presence of 10 μM heparin, in PBS buffer containing 1 mM DTT under continuous shaking (600 rpm) for 5 days at 37 °C in an Eppendorf Thermomixer. The quality of 1N4R tau fibrils produced after 5 days was assessed by ThioflavinT binding, sedimentation, and transmission electron microscopy (TEM). The resulting 1N4R tau fibrils were spun at 25 °C and 75 000 g for 30 min. The pelleted fibrils were resuspended in PBS buffer with 1 mM DTT at 50 μM equivalent monomeric tau concentration. 1N4R tau fibrils were labeled by incubation with the 2 molar equivalents of lysine-reactive ATTO 550 (ATTO-TEC, GMBH) for 1 h at room temperature. The unreacted fluorophore was removed by two cycles of centrifugation at 75 000 g for 10 min and resuspension of the pellet in PBS. 1N4R tau fibrils were fragmented by sonication for 5 min in 2-ml Eppendorf tubes in a Vial Tweeter powered by an ultrasonic processor UIS250v (250 W, 2.4 kHz; Hielscher Ultrasonic, Teltow, Germany) to generate

fibrillar particles with an average size 50 nm as assessed by TEM analysis. For seeding experiments, either monomeric or fibrillar tau was added directly into the cell culture media to a final concentration of 400 nM. Cells were then fixed after 48 hours.

Statistical analysis

Statistical analysis was performed with GraphPad Prism (GraphPad Software, Version 6h and 10.1.1). Data was tested for normal distribution by D'Agostino and Pearson omnibus normality test. Data presentation, sample size (number of biological repeats and sample size per repeat and condition), and the applied statistical tests are indicated in the figure legends for each experiment. For all cell culture data, data represents 3 independent replicates with 10 images each replicate. Significance levels: non-significant (n.s.) $p > 0.05$, $*p \leq 0.05$, $**p \leq 0.01$, and $***p \leq 0.001$.

Data availability

All data supporting the findings of this study are available within the paper and its supplementary information. *C. elegans* strains and plasmids generated in this study are available upon request.

Acknowledgements

We gratefully acknowledge the technical support of Sarah Wübbel. We extend our gratitude to Dr. Sunil Yeruva for his assistance with the use of the DMI6000 confocal microscope. We appreciate the help of Dr. Hana Nuskova and Dr. Aurelio Teleman (DKFZ, Heidelberg) with the fatty acid conjugation protocol. The tauP301S-Venus expressing HEK293T cell line was kindly provided by Dr. William A. McEwan (Cambridge University)[38]. The pLenti PGK Puro DEST (w529-2) vector was a gift from Dr. Eric Campeau and Dr. Paul Kaufman[62]. We also thank Dr. Bin Liu and Dr. Marja Jäättelä (University of Copenhagen) for sharing the strain BIJ34 and a pPD49.26 expression plasmid coding for sfGFP::LGALS3 and Dr. Xiaochen Wang (Chinese Academy of Sciences, Beijing) for nematodes expressing the qxIs352 transgene. Some strains were provided by the Caenorhabditis Genetics Center (CGC), which is funded by the NIH Office of Research Infrastructure Programs (P40 OD010440).

Additional information

Author contributions

Conceptualization J.T., C.A.S., C.N.K.

Formal Analysis J.T., C.A.S., N.M.

Funding acquisition R.M., C.N.K.

Investigation J.T., C.A.S., N.M., D.E.

Methodology J.T., C.A.S., N.M.

Project administration C.N.K.

Resources S.B.N.N.

Supervision R.M., C.N.K.

Visualization J.T., C.N.K.

Writing – original draft J.T., C.A.S., C.N.K.

Writing – review & editing J.T., C.A.S., N.M., D.E., R.M., C.N.K.

Additional files

Supplemental File

References

1. Clavaguera F., Bolmont T., Crowther R.A., Abramowski D., Frank S., Probst A., Fraser G., Stalder A.K., Beibel M., Staufenbiel M., et al. (2009) **Transmission and spreading of tauopathy in transgenic mouse brain** *Nat Cell Biol* **11**:909–913 https://doi.org/10.1038/ncb1901 | Google Scholar

2. Walker L.C., Jucker M (2024) **The prion principle and Alzheimer's disease** *Science* **385**:1278–1279 https://doi.org/10.1126/science.adq5252 | Google Scholar

3. Biel D., Brendel M., Rubinski A., Buerger K., Janowitz D., Dichgans M., Franzmeier N., Alzheimer's Disease Neuroimaging, I. (2021) **tau-PET and in vivo Braak-staging as prognostic markers of future cognitive decline in cognitively normal to demented individuals** *Alzheimer's research & therapy* **13**:137 https://doi.org/10.1186/s13195-021-00880-x | Google Scholar

4. Frost B., Jacks R.L., Diamond M.I (2009) **Propagation of tau misfolding from the outside to the inside of a cell** *J Biol Chem* **284**:12845–12852 https://doi.org/10.1074/jbc.M808759200 | Google Scholar

5. Sanders D.W., Kaufman S.K., DeVos S.L., Sharma A.M., Mirbaha H., Li A., Barker S.J., Foley A.C., Thorpe J.R., Serpell L.C., et al. (2014) **Distinct tau prion strains propagate in cells and mice and define different tauopathies** *Neuron* **82**:1271–1288 https://doi.org/10.1016/j.neuron.2014.04.047 | Google Scholar

6. Shrivastava A.N., Redeker V., Pieri L., Bousset L., Renner M., Madiona K., Mailhes-Hamon C., Coens A., Buee L., Hantraye P., et al. (2019) **Clustering of tau fibrils impairs the synaptic composition of alpha3-Na(+)/K(+)-ATPase and AMPA receptors** *EMBO J* **38** https://doi.org/10.15252/embj.201899871 | Google Scholar

7. Caballero B., Wang Y., Diaz A., Tasset I., Juste Y.R., Stiller B., Mandelkow E.M., Mandelkow E., Cuervo A.M (2018) **Interplay of pathogenic forms of human tau with different autophagic pathways** *Aging cell* **17** https://doi.org/10.1111/acel.12692 | Google Scholar

8. Menzies F.M., Fleming A., Rubinsztein D.C (2015) **Compromised autophagy and neurodegenerative diseases** *Nat Rev Neurosci* **16**:345–357 https://doi.org/10.1038/nrn3961 | Google Scholar

9. Nixon R.A., Wegiel J., Kumar A., Yu W.H., Peterhoff C., Cataldo A., Cuervo A.M (2005) **Extensive involvement of autophagy in Alzheimer disease: an immuno-electron microscopy study** *J Neuropathol Exp Neurol* **64**:113–122 Google Scholar

10. Hou W.C., Massey L.A., Rhoades D., Wu Y., Ren W., Frank C., Overkleeft H.S., Kelly J.W (2024) **A PIKfyve modulator combined with an integrated stress response inhibitor to treat lysosomal storage diseases** *Proc Natl Acad Sci U S A* **121**:e2320257121 https://doi.org/10.1073/pnas.2320257121 | Google Scholar

11. Lim S.H.Y., Hansen M., Kumsta C (2024) **Molecular Mechanisms of Autophagy Decline during Aging** *Cells* **13** https://doi.org/10.3390/cells13161364 | Google Scholar

12. Caballero B., Bourdenx M., Luengo E., Diaz A., Sohn P.D., Chen X., Wang C., Juste Y.R., Wegmann S., Patel B., et al. (2021) **Acetylated tau inhibits chaperone-mediated autophagy and promotes tau pathology propagation in mice** *Nature communications* **12**:2238 https://doi.org/10.1038/s41467-021-22501-9 | Google Scholar

13. Chen J.J., Nathaniel D.L., Raghavan P., Nelson M., Tian R., Tse E., Hong J.Y., See S.K., Mok S.A., Hein M.Y., et al. (2019) **Compromised function of the ESCRT pathway promotes endolysosomal escape of tau seeds and propagation of tau aggregation** *J Biol Chem* https://doi.org/10.1074/jbc.RA119.009432 | Google Scholar

14. Flavin W.P., Bousset L., Green Z.C., Chu Y., Skarpathiotis S., Chaney M.J., Kordower J.H., Melki R., Campbell E.M (2017) **Endocytic vesicle rupture is a conserved mechanism of cellular invasion by amyloid proteins** *Acta Neuropathol* https://doi.org/10.1007/s00401-017-1722-x | Google Scholar

15. Tuck B.J., Miller L.V.C., Katsinelos T., Smith A.E., Wilson E.L., Keeling S., Cheng S., Vaysburd M.J., Knox C., Tredgett L., et al. (2022) **Cholesterol determines the cytosolic entry and seeded aggregation of tau** *Cell reports* **39**:110776 https://doi.org/10.1016/j.celrep.2022.110776 | Google Scholar

16. Dimou E., Katsinelos T., Meisl G., Tuck B.J., Keeling S., Smith A.E., Hidari E., Lam J.Y.L., Burke M., Lovestam S., et al. (2023) **Super-resolution imaging unveils the self-replication of tau aggregates upon seeding** *Cell reports* **42**:112725 https://doi.org/10.1016/j.celrep.2023.112725 | Google Scholar

17. Polanco J.C., Hand G.R., Briner A., Li C., Götz J (2021) **Exosomes induce endolysosomal permeabilization as a gateway by which exosomal tau seeds escape into the cytosol** *Acta Neuropathol* **141**:235–256 https://doi.org/10.1007/s00401-020-02254-3 | Google Scholar

18. Rose K., Jepson T., Shukla S., Maya-Romero A., Kampmann M., Xu K., Hurley J.H (2024) **tau fibrils induce nanoscale membrane damage and nucleate cytosolic tau at lysosomes** *Proc Natl Acad Sci U S A* **121**:e2315690121 https://doi.org/10.1073/pnas.2315690121 | Google Scholar

19. Kroemer G., Jaattela M (2005) **Lysosomes and autophagy in cell death control** *Nature reviews. Cancer* **5**:886–897 https://doi.org/10.1038/nrc1738 | Google Scholar

20. Sandhof C.A., Martin N., Tittelmeier J., Schlueter A., Pezzali M., Schoendorf D.C., Lange T., Reinhardt P., Ried J.S., Liang S., et al. (2024) **A Novel C. elegans Model for tau Spreading Reveals Genes Critical for Endolysosomal Integrity and Seeded tau Aggregation** *bioRxiv* :2024.2011.2013.619586 https://doi.org/10.1101/2024.11.13.619586 | Google Scholar

21. Breslow D.K., Weissman J.S (2010) **Membranes in balance: mechanisms of sphingolipid homeostasis** *Mol Cell* **40**:267–279 https://doi.org/10.1016/j.molcel.2010.10.005 | Google Scholar

22. Jimenez-Rojo N., Leonetti M.D., Zoni V., Colom A., Feng S., Iyengar N.R., Matile S., Roux A., Vanni S., Weissman J.S., Riezman H (2020) **Conserved Functions of Ether Lipids and Sphingolipids**

in the Early Secretory Pathway *Curr Biol* **30**:3775–3787 https://doi.org/10.1016/j.cub.2020.07.059 | Google Scholar

23. Gault C.R., Obeid L.M., Hannun Y.A (2010) **An overview of sphingolipid metabolism: from synthesis to breakdown** *Adv Exp Med Biol* **688**:1–23 https://doi.org/10.1007/978-1-4419-6741-1_1 | Google Scholar

24. Futerman A.H., Hannun Y.A (2004) **The complex life of simple sphingolipids** *EMBO Rep* **5**:777–782 https://doi.org/10.1038/sj.embor.7400208 | Google Scholar

25. Czubowicz K., Jesko H., Wencel P., Lukiw W.J., Strosznajder R.P (2019) **The Role of Ceramide and Sphingosine-1-Phosphate in Alzheimer's Disease and Other Neurodegenerative Disorders** *Mol Neurobiol* **56**:5436–5455 https://doi.org/10.1007/s12035-018-1448-3 | Google Scholar

26. van Echten-Deckert G., Walter J. (2012) **Sphingolipids: critical players in Alzheimer's disease** *Prog Lipid Res* **51**:378–393 https://doi.org/10.1016/j.plipres.2012.07.001 | Google Scholar

27. Huotari J., Helenius A (2011) **Endosome maturation** *EMBO J* **30**:3481–3500 https://doi.org/10.1038/emboj.2011.286 | Google Scholar

28. Yong J., Villalta J.E., Vu N., Kukurugya M.A., Olsson N., Lopez M.P., Lazzari-Dean J.R., Hake K., McAllister F.E., Bennett B.D., Jan C.H (2024) **Impairment of lipid homeostasis causes lysosomal accumulation of endogenous protein aggregates through ESCRT disruption** *eLife* **12** https://doi.org/10.7554/eLife.86194 | Google Scholar

29. Aits S., Kricker J., Liu B., Ellegaard A.M., Hamalisto S., Tvingsholm S., Corcelle-Termeau E., Hogh S., Farkas T., Holm Jonassen A., et al. (2015) **Sensitive detection of lysosomal membrane permeabilization by lysosomal galectin puncta assay** *Autophagy* **11**:1408–1424 https://doi.org/10.1080/15548627.2015.1063871 | Google Scholar

30. Hanel V., Pendleton C., Witting M (2019) **The sphingolipidome of the model organism Caenorhabditis elegans** *Chem Phys Lipids* **222**:15–22 https://doi.org/10.1016/j.chemphyslip.2019.04.009 | Google Scholar

31. Cheng X., Jiang X., Tam K.Y., Li G., Zheng J., Zhang H (2019) **Sphingolipidomic Analysis of C. elegans reveals Development– and Environment-dependent Metabolic Features** *Int J Biol Sci* **15**:2897–2910 https://doi.org/10.7150/ijbs.30499 | Google Scholar

32. D'Auria L., Bongarzone E.R (2016) **Fluid levity of the cell: Role of membrane lipid architecture in genetic sphingolipidoses** *J Neurosci Res* **94**:1019–1024 https://doi.org/10.1002/jnr.23750 | Google Scholar

33. Liu B., Du H., Rutkowski R., Gartner A., Wang X (2012) **LAAT-1 is the lysosomal lysine/arginine transporter that maintains amino acid homeostasis** *Science* **337**:351–354 https://doi.org/10.1126/science.1220281 | Google Scholar

34. Morck C., Olsen L., Kurth C., Persson A., Storm N.J., Svensson E., Jansson J.O., Hellqvist M., Enejder A., Faergeman N.J., Pilon M (2009) **Statins inhibit protein lipidation and induce the unfolded protein response in the non-sterol producing nematode Caenorhabditis elegans** *Proc Natl Acad Sci U S A* **106**:18285–18290 https://doi.org/10.1073/pnas.0907117106 | Google Scholar

35. Owen D.M., Rentero C., Magenau A., Abu-Siniyeh A., Gaus K (2011) **Quantitative imaging of membrane lipid order in cells and organisms** *Nat Protoc* **7**:24–35 https://doi.org/10.1038/nprot.2011.419 | Google Scholar

36. Barucha-Kraszewska J., Kraszewski S., Ramseyer C (2013) **Will C-Laurdan dethrone Laurdan in fluorescent solvent relaxation techniques for lipid membrane studies?** *Langmuir* **29**:1174–1182 https://doi.org/10.1021/la304235r | Google Scholar

37. Wittrup A., Ai A., Liu X., Hamar P., Trifonova R., Charisse K., Manoharan M., Kirchhausen T., Lieberman J (2015) **Visualizing lipid-formulated siRNA release from endosomes and target gene knockdown** *Nat Biotechnol* **33**:870–876 https://doi.org/10.1038/nbt.3298 | Google Scholar

38. McEwan W.A., Falcon B., Vaysburd M., Clift D., Oblak A.L., Ghetti B., Goedert M., James L.C (2017) **Cytosolic Fc receptor TRIM21 inhibits seeded tau aggregation** *Proc Natl Acad Sci U S A* **114**:574–579 https://doi.org/10.1073/pnas.1607215114 | Google Scholar

39. Nachman E., Wentink A.S., Madiona K., Bousset L., Katsinelos T., Allinson K., Kampinga H., McEwan W.A., Jahn T.R., Melki R., et al. (2020) **Disassembly of tau fibrils by the human Hsp70 disaggregation machinery generates small seeding-competent species** *J Biol Chem* **295**:9676–9690 https://doi.org/10.1074/jbc.RA120.013478 | Google Scholar

40. Yoon J.H., Seo Y., Jo Y.S., Lee S., Cho E., Cazenave-Gassiot A., Shin Y.S., Moon M.H., An H.J., Wenk M.R., Suh P.G (2022) **Brain lipidomics: From functional landscape to clinical significance** *Sci Adv* **8**:eadc9317 https://doi.org/10.1126/sciadv.adc9317 | Google Scholar

41. Hornemann T (2021) **Mini review: Lipids in Peripheral Nerve Disorders** *Neurosci Lett* **740**:135455 https://doi.org/10.1016/j.neulet.2020.135455 | Google Scholar

42. Uranbileg B., Isago H., Sakai E., Kubota M., Saito Y., Kurano M (2024) **Alzheimer's disease manifests abnormal sphingolipid metabolism** *Front Aging Neurosci* **16**:1368839 https://doi.org/10.3389/fnagi.2024.1368839 | Google Scholar

43. Corder E.H., Saunders A.M., Strittmatter W.J., Schmechel D.E., Gaskell P.C., Small G.W., Roses A.D., Haines J.L., Pericak-Vance M.A (1993) **Gene dose of apolipoprotein E type 4 allele and the risk of Alzheimer's disease in late onset families** *Science* **261**:921–923 https://doi.org/10.1126/science.8346443 | Google Scholar

44. Kosicek M., Zetterberg H., Andreasen N., Peter-Katalinic J., Hecimovic S (2012) **Elevated cerebrospinal fluid sphingomyelin levels in prodromal Alzheimer's disease** *Neurosci Lett* **516**:302–305 https://doi.org/10.1016/j.neulet.2012.04.019 | Google Scholar

45. Ruiz M., Devkota R., Kaper D., Ruhanen H., Busayavalasa K., Radovic U., Henricsson M., Kakela R., Boren J., Pilon M (2023) **AdipoR2 recruits protein interactors to promote fatty acid elongation and membrane fluidity** *J Biol Chem* **299**:104799 https://doi.org/10.1016/j.jbc.2023.104799 | Google Scholar

46. Zhang Y., Wang H., Zhang J., Hu Y., Zhang L., Wu X., Su X., Li T., Zou X., Liang B (2016) **The cytochrome b5 reductase HPO-19 is required for biosynthesis of polyunsaturated fatty acids in Caenorhabditis elegans** *Biochim Biophys Acta* **1861**:310–319 https://doi.org/10.1016/j.bbalip.2016.01.009 | Google Scholar

47. Fabri J., de Sa N.P., Malavazi I., Del Poeta M. (2020) **The dynamics and role of sphingolipids in eukaryotic organisms upon thermal adaptation** *Prog Lipid Res* **80**:101063 https://doi.org/10

.1016/j.plipres.2020.101063 | Google Scholar

48. Romanauska A., Kohler A (2023) **Lipid saturation controls nuclear envelope function** *Nat Cell Biol* **25**:1290–1302 https://doi.org/10.1038/s41556-023-01207-8 | Google Scholar

49. Harayama T., Riezman H (2018) **Understanding the diversity of membrane lipid composition** *Nat Rev Mol Cell Biol* **19**:281–296 https://doi.org/10.1038/nrm.2017.138 | Google Scholar

50. Rakhra V., Galappaththy S.L., Bulchandani S., Cabandugama P.K (2020) **Obesity and the Western Diet: How We Got Here** *Mo Med* **117**:536–538 Google Scholar

51. Snowden S.G., Ebshiana A.A., Hye A., An Y., Pletnikova O., O'Brien R., Troncoso J., Legido-Quigley C., Thambisetty M (2017) **Association between fatty acid metabolism in the brain and Alzheimer disease neuropathology and cognitive performance: A nontargeted metabolomic study** *PLoS Med* **14**:e1002266 https://doi.org/10.1371/journal.pmed.1002266 | Google Scholar

52. Bischoff-Ferrari H.A., Gangler S., Wieczorek M., Belsky D.W., Ryan J., Kressig R.W., Stahelin H.B., Theiler R., Dawson-Hughes B., Rizzoli R., et al. (2025) **Individual and additive effects of vitamin D, omega-3 and exercise on DNA methylation clocks of biological aging in older adults from the DO-HEALTH trial** *Nat Aging* https://doi.org/10.1038/s43587-024-00793-y | Google Scholar

53. Shinto L., Quinn J., Montine T., Dodge H.H., Woodward W., Baldauf-Wagner S., Waichunas D., Bumgarner L., Bourdette D., Silbert L., Kaye J (2014) **A randomized placebo-controlled pilot trial of omega-3 fatty acids and alpha lipoic acid in Alzheimer's disease** *J Alzheimers Dis* **38**:111–120 https://doi.org/10.3233/JAD-130722 | Google Scholar

54. Wood A.H.R., Chappell H.F., Zulyniak M.A (2022) **Dietary and supplemental long-chain omega-3 fatty acids as moderators of cognitive impairment and Alzheimer's disease** *Eur J Nutr* **61**:589–604 https://doi.org/10.1007/s00394-021-02655-4 | Google Scholar

55. Brenner S (1974) **The genetics of Caenorhabditis elegans** *Genetics* **77**:71–94 Google Scholar

56. Svensk E., Stahlman M., Andersson C.H., Johansson M., Boren J., Pilon M (2013) **PAQR-2 regulates fatty acid desaturation during cold adaptation in C. elegans** *PLoS Genet* **9**:e1003801 https://doi.org/10.1371/journal.pgen.1003801 | Google Scholar

57. Devkota R., Svensk E., Ruiz M., Stahlman M., Boren J., Pilon M (2017) **The adiponectin receptor AdipoR2 and its Caenorhabditis elegans homolog PAQR-2 prevent membrane rigidification by exogenous saturated fatty acids** *PLoS Genet* **13**:e1007004 https://doi.org/10.1371/journal.pgen.1007004 | Google Scholar

58. Sandhof C.A., Hoppe S.O., Druffel-Augustin S., Gallrein C., Kirstein J., Voisine C., Nussbaum-Krammer C (2020) **Reducing INS-IGF1 signaling protects against non-cell autonomous vesicle rupture caused by SNCA spreading** *Autophagy* **16**:878–899 https://doi.org/10.1080/15548627.2019.1643657 | Google Scholar

59. Devkota R., Pilon M (2018) **FRAP: A Powerful Method to Evaluate Membrane Fluidity in Caenorhabditis elegans** *Bio Protoc* **8**:e2913 https://doi.org/10.21769/BioProtoc.2913 | Google Scholar

60. Svensk E., Devkota R., Stahlman M., Ranji P., Rauthan M., Magnusson F., Hammarsten S., Johansson M., Boren J., Pilon M (2016) **Caenorhabditis elegans PAQR-2 and IGLR-2 Protect against Glucose Toxicity by Modulating Membrane Lipid Composition** *PLoS Genet* **12**:e1005982 https://doi.org/10.1371/journal.pgen.1005982 | Google Scholar

61. Chalfie M., Sulston J.E., White J.G., Southgate E., Thomson J.N., Brenner S (1985) **The neural circuit for touch sensitivity in Caenorhabditis elegans** *J Neurosci* **5**:956–964 Google Scholar

62. Campeau E., Ruhl V.E., Rodier F., Smith C.L., Rahmberg B.L., Fuss J.O., Campisi J., Yaswen P., Cooper P.K., Kaufman P.D (2009) **A versatile viral system for expression and depletion of proteins in mammalian cells** *PLoS One* **4**:e6529 https://doi.org/10.1371/journal.pone.0006529 | Google Scholar

63. Jeong J.H., Han J.S., Jung Y., Lee S.M., Park S.H., Park M., Shin M.G., Kim N., Kang M.S., Kim S., et al. (2023) **A new AMPK isoform mediates glucose-restriction induced longevity non-cell autonomously by promoting membrane fluidity** *Nature communications* **14** https://doi.org/10.1038/s41467-023-35952-z | Google Scholar

64. Oliveira A.F., Cunha D.A., Ladriere L., Igoillo-Esteve M., Bugliani M., Marchetti P., Cnop M (2015) **In vitro use of free fatty acids bound to albumin: A comparison of protocols** *Biotechniques* **58**:228–233 https://doi.org/10.2144/000114285 | Google Scholar

65. Cousin S.P., Hugl S.R., Wrede C.E., Kajio H., Myers M.G., Rhodes C.J (2001) **Free fatty acid-induced inhibition of glucose and insulin-like growth factor I-induced deoxyribonucleic acid synthesis in the pancreatic beta-cell line INS-1** *Endocrinology* **142**:229–240 https://doi.org/10.1210/endo.142.1.7863 | Google Scholar

66. Nuskova H., Cortizo F.G., Schwenker L.S., Sachsenheimer T., Diakonov E.E., Tiebe M., Schneider M., Lohbeck J., Reid C., Kopp-Schneider A., et al. (2023) **Competition for cysteine acylation by C16:0 and C18:0 derived lipids is a global phenomenon in the proteome** *J Biol Chem* **299**:105088 https://doi.org/10.1016/j.jbc.2023.105088 | Google Scholar

67. Tardivel M., Begard S., Bousset L., Dujardin S., Coens A., Melki R., Buee L., Colin M (2016) **Tunneling nanotube (TNT)-mediated neuron-to neuron transfer of pathological tau protein assemblies** *Acta neuropathologica communications* **4** https://doi.org/10.1186/s40478-016-0386-4 | Google Scholar

68. Chitwood D.J., Lusby W.R., Thompson M.J., Kochansky J.P., Howarth O.W (1995) **The glycosylceramides of the nematode Caenorhabditis elegans contain an unusual, branched-chain sphingoid base** *Lipids* **30**:567–573 https://doi.org/10.1007/BF02537032 | Google Scholar

69. Zhang H., Abraham N., Khan L.A., Hall D.H., Fleming J.T., Gobel V (2011) **Apicobasal domain identities of expanding tubular membranes depend on glycosphingolipid biosynthesis** *Nat Cell Biol* **13**:1189–1201 https://doi.org/10.1038/ncb2328 | Google Scholar

70. Zhu H., Shen H., Sewell A.K., Kniazeva M., Han M (2013) **A novel sphingolipid-TORC1 pathway critically promotes postembryonic development in Caenorhabditis elegans** *eLife* **2**:e00429 https://doi.org/10.7554/eLife.00429 | Google Scholar

71. Scholz J., Helmer P.O., Nicolai M.M., Bornhorst J., Hayen H (2021) **Profiling of sphingolipids in Caenorhabditis elegans by two-dimensional multiple heart-cut liquid chromatography – mass spectrometry** *J Chromatogr A* **1655**:462481 https://doi.org/10.1016/j.chroma.2021.462481 | Google Scholar

Author information

Jessica Tittelmeier

Chair of Neuroanatomy, Institute of Anatomy, Faculty of Medicine, Ludwig-Maximilians University of Munich (LMU), Munich, Germany
ORCID iD: 0000-0002-8202-3702

Carl Alexander Sandhof

Center for Molecular Biology of Heidelberg University (ZMBH) and German Cancer Research Center (DKFZ), DKFZ-ZMBH Alliance, Heidelberg, Germany, Chemical Neurobiology Laboratory, Center for Genomic Medicine, Departments of Neurology and Psychiatry, Massachusetts General Hospital and Harvard Medical School, Boston, United States
ORCID iD: 0000-0001-8692-6987

Nicole Martin

Chair of Neuroanatomy, Institute of Anatomy, Faculty of Medicine, Ludwig-Maximilians University of Munich (LMU), Munich, Germany

Deike El-Kabarity

Chair of Neuroanatomy, Institute of Anatomy, Faculty of Medicine, Ludwig-Maximilians University of Munich (LMU), Munich, Germany

Soki-Bradel Ngonza-Nito

Institute Francois Jacob (MIRCen), CEA, and Laboratory of Neurodegenerative Diseases, CNRS, Fontenay-Aux-Roses, France

Ronald Melki

Institute Francois Jacob (MIRCen), CEA, and Laboratory of Neurodegenerative Diseases, CNRS, Fontenay-Aux-Roses, France

Carmen Nussbaum-Krammer

Chair of Neuroanatomy, Institute of Anatomy, Faculty of Medicine, Ludwig-Maximilians University of Munich (LMU), Munich, Germany, Center for Molecular Biology of Heidelberg University (ZMBH) and German Cancer Research Center (DKFZ), DKFZ-ZMBH Alliance, Heidelberg, Germany
ORCID iD: 0000-0002-8689-1363

For correspondence: carmen.nussbaum@med.uni-muenchen.de

Editors

Reviewing Editor
Ellen Nollen
University of Groningen, Groningen, Netherlands

Senior Editor
David Ron
University of Cambridge, Cambridge, United Kingdom

Reviewer #1 (Public review):

Summary:

In this study, Tittelmeier et al. explored the role of sphingolipid metabolism in maintaining endolysosomal membrane integrity and its downstream effects on tau aggregation and toxicity, using both worms and human cell models. The authors showed that knockdown of sphingolipid metabolism genes reduced endolysosomal membrane fluidity, as revealed by FRAP and C-Laurdan imaging, leading to increased vesicle rupture. Furthermore, tau aggregates accumulated in endolysosomes and exacerbated membrane rigidity and damage, promoting seeded tau aggregation, likely by enabling tau seed escape into the cytosol. Importantly, unsaturated fatty acid supplementation restored membrane fluidity, suppressed tau propagation, and alleviated neurotoxicity in *C. elegans*. These findings provide insight into how lipid dysregulation contributes to tau pathology and highlight membrane fluidity restoration as a potential therapeutic avenue for Alzheimer's disease.

Strengths:

The study addresses the connection between sphingolipid metabolism, endolysosomal membrane integrity, and tau pathology, which is a relevant topic in the context of Alzheimer's disease and related tauopathies.

The use of both C. elegans and human cell models provides cross-species perspectives that help frame the findings in a broader biological context.

The combination of FRAP and C-Laurdan dye imaging offers a biophysical approach to investigate changes in membrane properties, which is a technically interesting aspect of the study.

The observation that unsaturated fatty acid supplementation can modulate membrane fluidity and influence tau-related phenotypes adds an element of potential therapeutic interest.

The study presents multiple experimental approaches to address the proposed mechanism, and efforts were made to examine both membrane behavior and tau aggregation dynamics.

Weaknesses:

In Figure 3, the authors used C-Laurdan imaging to assess membrane fluidity and showed that knockdown of SPHK2, the human ortholog of sphk-1, led to increased membrane rigidity. However, the authors did not co-stain with a lysosomal marker, making it unclear whether the observed effect is specific to lysosomal membranes or reflects general membrane changes. Co-staining with LysoTracker or applying segmentation masks to isolate lysosomal signals would significantly improve interpretation.

Line 173 states that Lipofectamine 2000 increases membrane fluidity based on GP index changes, but this is incorrect. A higher GP index indicates increased membrane order (i.e., reduced fluidity), so the statement should be revised. Additionally, Lipofectamine 2000 can itself alter membrane rigidity, posing a risk of false-positive interpretations. To confirm the role of SPHK2 in this phenotype, the authors should use a CRISPR/Cas9 knockout model instead of relying solely on siRNA transfection, which may be confounded by the delivery reagent. Without lysosomal co-staining and SPHK2 KO validation, the authors cannot conclusively claim that SPHK2 loss affects endolysosomal membrane integrity.

The section titled "Fibrillar tau increases membrane rigidity and exacerbates endolysosomal damage" (lines 177-215) requires substantial revision. The narrative jumps abruptly between worms and cell models, making it hard to follow the logic. The use of the F3ΔK281::mCherry

strain is introduced without explanation or context. It is unclear whether this strain is relevant to lysosomal membrane rupture, as no reference or justification is provided. The authors should clarify whether this reporter is intended to detect lysosomal membrane permeabilization (LMP). If so, it would be more appropriate to use established LMP reporters, such as lysosome-targeted fluorescent sensors, galectin-based reporters, or dextran leakage assays. Based on the current data in Figure 3G, it is difficult to draw firm conclusions regarding membrane rupture levels.

To support the conclusion that sphingolipid metabolism gene knockdown alters membrane properties, the study would benefit from direct lipidomic analysis. Measuring changes in sphingolipid profiles in both C. elegans and cell models would provide biochemical evidence for the proposed disruption of lipid homeostasis. Given the availability of lipidomics platforms, this type of analysis should be feasible in both worms and human cells and would significantly strengthen the mechanistic claims regarding membrane fluidity and integrity.

The conclusions of the study rely heavily on imaging-based assays, including FRAP, C-Laurdan, and fluorescence microscopy. While these approaches provide valuable spatial and qualitative insights, they are inherently indirect and subject to interpretive limitations. To strengthen the mechanistic claims, the authors should incorporate additional biochemical or quantitative approaches. For example, lipidomics would allow direct measurement of membrane lipid composition changes, and western blotting or quantitative proteomics could assess levels of membrane-associated proteins involved in endolysosomal function or stress responses. Including such data would significantly improve the robustness and reproducibility of the study's conclusions.

The human cell experiments were performed exclusively in HEK293T cells, which are not physiologically relevant for modeling Alzheimer's disease or lysosomal function in neurons. Given that the study aims to draw conclusions related to tau aggregation and lysosomal membrane integrity, the use of a more disease-relevant cellular model is essential. There are several established AD-relevant cell models, including iPSC-derived neurons, neuroblastoma lines expressing tau, or microglial models, which would better reflect the cellular context of tauopathies. Validation of key findings in at least one of these systems would substantially enhance the biological relevance and translational impact of the study.

The authors reported that PUFA supplementation rescues neurotoxic phenotypes by increasing membrane fluidity. However, the data supporting this claim rely entirely on confocal imaging, shown in both the main and supplemental figures. To substantiate the mechanistic link between PUFA treatment and improved lysosomal membrane properties, the authors should include functional assays demonstrating that PUFAs are indeed incorporated into lysosomal membranes. Additionally, lipidomics analysis would be valuable to identify which lipid species are altered upon supplementation and correlate these changes with the observed phenotypic rescue. Furthermore, the conclusion that PUFAs rescue "neurotoxic phenotypes" is not appropriate based on data derived solely from HEK293T cells, which are not neuronal. To make claims about tau-related neurotoxicity, the authors should validate their findings in a more relevant neuronal model, such as SH-SY5Y neuroblastoma cells expressing tau or iPSC-derived neurons. This would better reflect the cellular environment of Alzheimer's disease and provide stronger support for the proposed therapeutic potential of PUFA supplementation.

While the authors demonstrate that ALA supplementation mitigates neurotoxicity in C. elegans expressing aggregated tau (F3ΔK281::mCherry), the current data are not sufficient to conclude that ALA directly rescues tau aggregation toxicity via a lysosome-specific mechanism. It remains unclear how lipid composition is altered upon ALA treatment and whether these changes correlate with functional improvement of lysosomal pathways. The manuscript does not provide mechanistic insight into how ALA enhances lysosomal health or attenuates endolysosomal damage. Moreover, supplementation with PUFAs like ALA can

activate a wide range of cellular processes beyond lysosomal function, including alterations in membrane fluidity, signaling cascades, and oxidative stress responses. The authors should clarify how they distinguish the lysosome-related effects from these alternative pathways. For example, did they observe specific lysosomal markers or structural improvements in lysosomes upon ALA treatment? Additional data or controls would be necessary to support a lysosome-specific protective mechanism and to exclude the involvement of other PUFA-responsive pathways in the observed phenotypes.

https://doi.org/10.7554/eLife.106865.1.sa2

Reviewer #2 (Public review):

Tittelmeier et al. investigated the role of sphingolipid (SL) metabolism in the maintenance of endolysosomal vesicle integrity. They find that both impaired SL biosynthesis and degradation in *C. elegans*, decrease the fluidity of endolysosomal membranes and promote their rupture, while it has little effect on plasma membrane fluidity. Endolysosomal membrane fluidity is also negatively affected in human cells upon knockdown (KD) of a gene (SPHK2) involved in the SL degradation pathway. Aggregated forms of tau in both models (*C. elegans* and human cells) can also cause rigidification of the endolysosomal membrane, with SL homeostasis disruption having an additive effect, exacerbating endolysosomal rupture. Notably, KD of SPHK2 also increased the formation of tau foci, suggesting that compromised endolysosomal integrity may promote tau aggregation. These data provide a clearer understanding of how genetic manipulation of SL metabolism affects endolysosomal membranes and their rigidification in the context of tau aggregation. Supplementation of polyunsaturated fatty acids (PUFAs), which has a beneficial effect on Alzheimer's patients, improved membrane fluidity and reduced tau propagation in human cells and tau-associated neurotoxicity in *C. elegans*, suggesting a possible mechanism of action.

Overall, the conclusions of this paper are supported by the data, with a few aspects requiring further clarification and elaboration.

(1) A reference to Figure S2E-G, which shows that KD of SL biosynthesis genes do not affect the plasma membrane, is missing from the main text.

(2) In Figure 3C, lipofectamine alone shows that it increases membrane rigidity (increased GP values), not membrane fluidity.

(3) In Figure 3F, the EV cntl condition expressing F3:mCh tau should have increased LGALS3 foci compared to the mCh EV cntl according to Ref (20) and its Figure 2G (at least for Day 5 animals), which would be indicative of the tau spreading in hypodermal tissue. What C. elegans age was examined in Figure 3F? Can the authors provide evidence of the transmission of the F3:mCh tau from the touch receptor neurons to the hypodermis in the EV [similar to Figure 2C & D from Ref (20)] and compare it to the KDs? Otherwise, it seems that KD of SL genes impacts not only endolysosomal rupture but significantly affects tau accumulation/spreading as well (e.g., shown later in HEK cells, where SPHK2 KD increases the formation of tau-Venus foci).

(4) Sphingolipids are essential membrane components and signaling molecules. Does KD of SL genes in C. elegans and the subsequent endolysosomal rupture cause any major, intermediate, or minor defects/phenotypes (in non-aggregation prone models, w/t..)?

https://doi.org/10.7554/eLife.106865.1.sa1

Reviewer #3 (Public review):

Summary:

The authors set off with an analysis of the lysosomal integrity upon knockdown of genes of the sphingolipid metabolic pathway that they identified in a previous (yet unpublished) work of an RNA screen using a new *C. elegans* Tau model. They then used cell culture and *C. elegans* experiments to study the link between lysosomal rupture and Tau propagation.

Strengths:

The authors use two complementary model systems and use probes to assess membrane rigidity that allow a quick assessment of the membrane dynamics and offer the opportunity to treat the cells with lipids, RNAi. Tau seeds, etc.

Weaknesses:

The main weakness is that this work builds on not-yet-peer-reviewed manuscript that established a new C. elegans Tau model and RNAi screen that aimed to identify genes involved in the propagation of Tau.

This reviewer misses essential information of the *C. elegans* Tau strain (not included in the method section): e.g., promoter used for the expression, information on the used Tau variant, expression pattern, and aggregation, etc.

Throughout the study, I missed data on:

(1) Effect of the knockdown on Tau expression, localisation (with lysosomal membrane?), aggregation, and proteotoxicity. The effect of the RNAi-mediated knockdown could also simply lead to a reduced expression of Tau that, in turn, leads to suppressed propagation.

(2) A quantification of RNAi knockdown is needed to judge the efficiency of the RNAi, in particular for the combinatorial RNAi experiments involving 2 and even 4 genes in parallel. Ideally, these analyses should be validated with mutants for these genes.

Further:

(3) Figure 4 H, I: Would Tau also aggregate in the absence of externally added Tau?

(4) How specific is the effect for Tau? It would help if the authors could assess other amyloid proteins.

(5) The connection between sphingolipids and AD is not new. See He et al, 2010, Neurobiol. Aging + numerous publications and also not between Tau seeding and lysosomal rupture: Rose et al., PNAS 2024 (that has been cited by the authors).

https://doi.org/10.7554/eLife.106865.1.sa0